Quaternary Science Reviews 250 (2020) 106655

Contents lists available at ScienceDirect

Quaternary Science Reviews

journal homepage: www.elsevier.com/locate/quascirev

Climate changes in Northeastern Brazil from deglacial to Meghalayan periods and related environmental impacts

Giselle Utida [a, *], Francisco W. Cruz [a], Roberto V. Santos [b], André O. Sawakuchi [a], Hong Wang [c], Luiz C.R. Pessenda [d], Valdir F. Novello [a], Mathias Vuille [e], André M. Strauss [f], Ana Claudia Borella [f], Nicolás M. Stríkis [g], Carlos C.F. Guedes [h], Fábio Ramos Dias De Andrade [a], Haiwei Zhang [i], Hai Cheng [i, j, k], R. Lawrence Edwards [l]

[a] Instituto de Geociências, Universidade de São Paulo, Rua do Lago, 562, Cidade Universitária, São Paulo, SP, 05508-090, Brazil
[b] Departamento de Geologia, Universidade de Brasília, Brasília, Brazil
[c] Interdisciplinary Research Center of Earth Science Frontier, Beijing Normal University, Beijing, China
[d] Universidade de São Paulo, 14C Laboratory, Piracicaba, SP, Brazil
[e] Department of Atmospheric and Environmental Sciences University at Albany, SUNY, Albany, NY, USA
[f] Museu de Arqueologia e Etnologia, Universidade de São Paulo, São Paulo, Brazil
[g] Departamento de Geoquímica, Universidade Federal Fluminense, Niterói, RJ, Brazil
[h] Departamento de Geologia, Universidade Federal do Paraná, Curitiba, Brazil
[i] Institute of Global Environmental Change, Xi'an Jiaotong University, Xi'an, 710054, China
[j] State Key Laboratory of Loess and Quaternary Geology, Institute of Earth Environment, Chinese Academy of Sciences, Xi'an, 710061, China
[k] Key Laboratory of Karst Dynamics, MLR, Institute of Karst Geology, CAGS, Guilin, 541004, China
[l] Department of Earth Sciences, University of Minnesota, Minneapolis, MN, USA

ARTICLE INFO

Article history:
Received 23 March 2020
Received in revised form
9 October 2020
Accepted 12 October 2020
Available online xxx

Keywords:
Stable isotopes
ITCZ
Speleothems
Holocene
Northeastern Brazil
Archaeology
Demographic impacts

ABSTRACT

Changes in insolation driven by precession and obliquity are considered the major driver of tropical precipitation on orbital time scales, and responsible for vegetation and physical landscape changes during the Late Holocene over tropical South America. Here we investigate the environmental changes in the karst region of Chapada do Apodi - Northeastern Brazil (NEB), using a multi-proxy approach including carbon ($\delta^{13}C$), oxygen ($\delta^{18}O$) and strontium ($^{87}Sr/^{86}Sr$) isotopic analyses on speleothems from different caves, carbonate bedrock, and clastic cave deposits. This approach reveals that the balance between soil formation and erosion and their alternating impact on vegetation and precipitation changes occurred in response to variations in the position and intensity of the Intertropical Convergence Zone (ITCZ) over the region. The high $\delta^{13}C$ and $\delta^{18}O$ and low $^{87}Sr/^{86}Sr$ values at 4,200 yrs BP indicate a massive episode of soil erosion, resulting in the exposure of carbonate bedrocks over a large area of the karst terrain. This event marks the beginning of the Meghalayan chronozone, characterized as the aridification of this region, decline in soil production, drying out of underground drainages, and increased dominance of dry-adapted flora species, characteristic of a more open vegetation (caatinga). We investigated if the Holocene climatic changes affected human occupation in the NEB and found that the overall demographic course is virtually identical to the well-established curve characterized by population deflation during Middle Holocene.

Authors statement

Giselle Utida: Conceptualization, Methodology, Formal analysis, Investigation, Writing - original draft. Francisco W. Cruz: Conceptualization, Methodology, Writing - original draft, Supervision, Funding acquisition. Roberto V. Santos: Resources, Writing - review & editing, Supervision. André O. Sawakuchi: Resources, Writing - review & editing, Supervision. Nicolas M. Stríkis: Writing - review & editing. Valdir F. Novello: Writing - review & editing. Hong Wang: Resources, Writing - review & editing, Supervision. Luiz Carlos R. Pessenda: Resources, Writing - review & editing, Supervision. Mathias Vuille: Writing - review & editing,

* Corresponding author.
E-mail address: giselleutida@hotmail.com (G. Utida).

https://doi.org/10.1016/j.quascirev.2020.106655
0277-3791/

Abbreviations

NEB	Northeastern Brazil
RN	speleothems isotopic dataset from Rio Grande do Norte state, Brazil
ITCZ	Intertropical Convergence Zone
LGM	Last Glacial Maximum
HS1	Heinrich Stadial 1
YD	Younger Dryas
OSL	Optically Stimulated Luminescence dating
OM	organic matter

Supervision. André Strauss: Methodology, Formal analysis, Writing - review & editing, Supervision. Ana Claúdia Borella: Methodology, Formal analysis, Writing - review & editing. Carlos C.F. Guedes: Resources, Writing - review & editing. Fábio R.D. de Andrade: Resources, Writing - review & editing. Haiwei Zhang: Resources, Writing - review & editing. Hai Cheng: Resources, Writing - review & editing, Supervision. R. Lawrence Edwards: Resources, Writing - review & editing, Supervision.

1. Introduction

Orbital forcing is thought to be a major driver of tropical precipitation in South America at time scales of thousands of years (Cruz et al., 2005, 2009; Braconnot et al., 2008; Cheng et al., 2013a; Prado et al., 2013). These changes in precipitation are associated with rainforest retraction and expansion and changes in vegetation types since the Last Glacial Maximum (LGM) in tropical South America (Mayle et al., 2000; Ledru et al., 2009; Novello et al., 2019; Pinaya et al., 2019). However, a careful look at the paleoclimate records (e.g. Cruz et al., 2009; Novello et al., 2017; Strikis et al., 2018) reveals that observed changes in the hydrologic regime occur at a much faster rate than the orbital forcing, suggesting that the climate system was forced to cross a threshold that triggered a transition of the global monsoon circulation to a new state (Alley et al., 2003).

During the Holocene, an abrupt climate transition at 4,200 yrs BP marks the base of the Meghalayan chronozone, a period of aridification in the mid and low-latitudes. Officially the 4.2 ka event is defined as a shift to heavier δ^{18}Ovalues in an Indian speleothem record, that marks the abrupt climatic transition from Middle to Late Holocene (Berkelhammer et al., 2012; Walker et al., 2012, 2018). Most of the records indicate the abrupt onset of aridification in the Mediterranean region and parts of Asia, North America and Africa (e.g., Thompson et al., 2002; Booth et al., 2005; Dixit et al., 2014; Cheng et al., 2015; Kaniewski et al., 2017; Bini et al., 2019; Toth and Aronso, 2019). In Northeastern Brazil, the 4.2 ka event is marked by the onset of drier conditions (De Oliveira et al., 1999; Zular et al., 2018).

The global forcing mechanisms that led to the 4.2 ka event are still not understood, but have been linked to the changes in orbital forcing (Cruz et al., 2009; Liu and Feng, 2012), southward migration of the Intertropical Convergence Zone (ITCZ) (Zanchetta et al., 2016; Zhang et al., 2020), changes in North Atlantic surface waters (Bond et al., 1997; Zhang et al., 2018; Isola et al., 2019; Bini et al., 2019) and the variability of the El Niño - Southern Oscillation (Fisher, 2011; Gen et al., 2020; Dang et al., 2020).

However, despite its impacts on climate worldwide, the global expression of the transition to the Meghalayan remains unexplored, and its significance has not yet been studied in most parts of South America, although many proxy records point to significant environmental changes after the 4.2 ka event.

At the time of transition to the Meghalayan chronozone, speleothems from NEB experienced a rapid enrichment in δ^{18}O values, indicative of an abrupt precipitation reduction, antiphased with the rest of tropical South America since the Last Glacial Maximum (Cruz et al., 2009). This occurs near the inflection point of the precessional forcing curve and the enriched oxygen isotopes in speleothems persisted during the last 4,200 years (Cruz et al., 2009). The drier climate in NEB is widely confirmed by pollen records showing a change toward vegetation adapted to drier climate in parallel with the austral summer insolation increasing after 4,200 yrs BP (De Oliveira et al., 1999; Montade et al., 2014).

Thus, understanding how orbitally driven precipitation changes have affected the vegetation and Earth surface processes, such as soil denudation, is critical to assess the tropical ecosystem's resilience to natural climate oscillations. Furthermore, the aridification trend that started at about 4,200 yrs BP impacted human societies and in some cases even led to their collapse. For instance, there is evidence that agricultural societies around the world were affected, resulting in regional abandonments (e.g. Liu and Feng, 2012; Torrescano-Valle and Islebe, 2015; Weiss, 2016; Kaniewski et al., 2017; Ran and Chen, 2019). In South America, there is some evidence pointing to similar impacts as a consequence of hydroclimate variability during the Middle Holocene across the continent (Riris and Arroyo-Kalin, 2019). However, these conclusions might not be valid for NEB given that this region experienced a climate response that was antiphased with most of the region within the South American Monsoon domain (Cheng et al., 2013a).

The combined application of carbon and strontium isotope ratios in speleothem records has been used as an important tool to understand the relationship between local hydrology, host-rock dissolution, and rate of soil production/erosion (Ward et al., 2019; Novello et al., 2019). These studies have investigated the contribution of distinct sources of strontium to the isotopic signals embedded in the speleothems, such as soil and sediments overlying the cave surface and bedrock. This kind of study can help to understand the relative contribution of each strontium source that is regulated by processes such as precipitation amount, soil production/erosion, changes in vegetation coverage, leaching, and rock dissolution.

Strontium isotopes are a valuable tool because the weathering is the main mechanism that transfers the strontium from rocks to the hydrological cycle with low fractionation factors, and the chemical reactions vary as a function of environmental and rock conditions (Banner, 2004). They act as efficient trackers of sediment sources and soil-erosion dynamics (Frumkin and Stein, 2004; Cooke, 2003; Li, 2005; Zhou et al., 2009). Speleothem $^{87}Sr/^{86}Sr$ ratios record the Sr isotopic composition of cave water and its variations reflect changes in the relative contribution of distinct Sr sources, as soil and bedrock. When sources have different $^{87}Sr/^{86}Sr$ signatures, they may act as end-members for interpretation of the speleothem Sr composition, as described in previous studies that were performed in Brazilian caves (Wortham et al., 2017; Novello et al., 2019).

Speleothem δ^{13}C values are considered more complex and can be ultimately affected by processes that took place in the soil and in the epikarst zone (Meyers et al., 2014; Wong and Breecker, 2015). Changes in vegetation cover and soil productivity above the cave control the speleothem δ^{13}C variations. The predominance of C3 plants results in stalagmite δ^{13}C values of −14‰ to −6‰, while under the predominance of C4 plants, stalagmite δ^{13}C values vary from −6‰ to +2‰, considering carbonate bedrock with a δ^{13}C value of +1‰ in both cases (Hendy, 1971; Baker, 1997; McDermott, 2004). Other processes that can affect the δ^{13}C of the speleothems include changes in the atmospheric δ^{13}C and pCO_2 (Schubert and

Jahren, 2012), and rate of degassing of CO_2 during calcite deposition under the epikarst and inside caves driven by cave atmosphere pCO_2 (Drybrodt, 2008; Dreybrodt and Scholz, 2011; Feng et al., 2012; Mickler et al., 2004). While the diversity of mechanisms that control the speleothem carbon isotope composition make the environmental interpretation more complex, some studies have demonstrated that soil processes exert a dominant control on the speleothem $\delta^{13}C$ signal (Cruz et al., 2006; Novello et al., 2019, 2020).

In addition, the association between strontium and carbon isotopes in the same speleothems can be a reliable indicator of relative soil coverage and vegetation density above the cave, controlled by hydrological fluctuations (Novello et al., 2019; Ward et al., 2019). Enriched (depleted) $^{87}Sr/^{86}Sr$ signals represent an increased (decreased) soil contribution relative to the bedrock, while depleted (enriched) $\delta^{13}C$ values indicate a predominantly denser (sparser) vegetation signal (Novello et al., 2019).

In this context, we developed a multi-proxy study in the karst region of Chapada do Apodi in NEB, based on $\delta^{13}C$ and $^{87}Sr/^{86}Sr$ in host-rock and in the sedimentary deposits from the Urubu Cave, and together with $\delta^{13}C$ and $\delta^{18}O$ records in stalagmites from the nearby caves of Rainha, Abissal and Trapiá. This multi-proxy approach allows us to identify the shifts in soil dynamics, cave infilling, and the development of karst pavement associated with paleo-precipitation and vegetation changes in NEB from Heinrich Stadial 1 (HS1), defined from 17,300 to 15,100 yrs BP, according to NEB speleothems isotopic record (Cruz et al., 2009), to the Meghalayan Age. Moreover, we discuss the possible implications of the paleoenvironmental changes on the human occupation in the region during the Holocene.

2. Regional settings

The study area is located in the Rio Grande do Norte State, a region at the edge of NEB (Fig. 1). The annual mean temperature is around 28 °C (INMET - National Institute of Meteorology – Instituto Nacional de Meteorologia – data from 1961 to 1990). Average precipitation is approximately 730 mm/year and it is concentrated in the period when the ITCZ migrates to the south, between March and May with ca. 150 mm for this period (Fig. 1a) (Agência Nacional de Águas – ANA - National Agency of Waters, 2013; Ziese et al., 2018). In the wettest years, the rainy season starts earlier in January/February, with ca. 108 mm/month, also originated from southward shift of the ITCZ. The smallest precipitation contribution occurs from June to January with ca. 20 mm/month (Fig. 1a).

The typical vegetation in the region is the caatinga, a dry forest adapted to the semi-arid climate and characterized by sparse vegetation dominated by arboreal deciduous scrubland (Fig. 1b) (Ab'Saber, 1974; Leal et al., 2005). Differently from Brazilian Savanna vegetation, or Brazilian cerrado, the caatinga is well adapted to short rainy seasons of 3–4 months in length and tolerates large interannual variations in precipitation that are strongly influenced by El Niño and La Niña events (Prado, 2003; Erasmi et al., 2009).

The regional karst is developed in Cretaceous carbonate rocks of the Jandaíra Formation, Potiguar Basin (Pessoa-Neto, 2003; Angelim et al., 2006; Melo et al., 2016). The caves were developed close to the Apodi River valley and off cliffs that define a carbonate *cuesta* along the contact between carbonate rocks and sandstone units from the Cretaceous Jandaíra and Açu Formations, respectively (Fig. 2).

The karst pavements, locally called Lajedos (Porpino et al., 2009; Cruz Júnior, 1996), comprise large areas that are several km long, with dense occurrence of solutional and collapsed features that are preferentially developed in the proximity of the riverbanks (Fig. 2b). A substantial number of small canyon-like caves, which developed along enlarged fractures and bedding planes, are usually observed at depths of less than 40 m (Silva et al., 2017). A small number of caves are longer than a few hundred meters and consist of non-active underground drainages that flow toward the Apodi River. Although the soil cover is very sparse and almost absent at the surface of the studied caves (Fig. 2b), the cave galleries, fractures, and sinkholes are commonly clogged with clastic sediments interpreted as result of soil erosion by surface water run-off and cave rivers. The relict soils over the karst pavements are characterized by a thin discontinuous cover of *Terra Rossa* soil, a reddish soil formed by chemical weathering of carbonate rocks during wet and warm periods (Choquette and James, 1988; Merino and Banerjee, 2008). Along the left margin of the Apodi River (Fig. 2), they are predominantly chernosoils, while on the right margin they are cambisoils (Embrapa Solos, 2006).

2.1. Cave deposits

At the study site, most cave entrances are located in an area locally known as Lajedos that are the highest areas of denudation of carbonate rocks (Fig. 2). We present data from speleothems collected in Rainha, Abissal and Trapiá caves, and clastic sediments and bat guano deposits from Urubu Cave (Fig. 3). All these caves are located within a radius of 6 km from 5°35′48.32"S and 37°41′51.04"W. Speleothems were found in Rainha and Trapiá Cave at about 150 and 500 m from their entrances. The latter is the largest cave system in the region with 2.3 km of passages (Zogbi et al., 2013). Rainha and Urubu caves are part of the same underground drainage, although they are not connected because clastic sediments block the passage between the two caves (Fig. 2a). Urubu Cave has around 30 m of linear extension and has two major salons connected by two channels, in different levels. A 1–2 m sequence of fine-grained clastic sediments underlying bat guano deposits is exposed in the lower passages of Urubu Cave. The guano consists of a 1–3 m thick layer found in both the lower and upper passages (Fig. 3b and c). The clastic sediment deposits are massive and show no apparent paleocurrent structures that could indicate flow direction as seen in other caves (Herman et al., 2012; González-Lemos et al., 2015).

The pile of guano was deposited after the cave drainage become inactive, as otherwise it would be totally eroded. Thousands of bats with different trophic levels (frugivorous, insectivorous and hematophagous) still inhabit the cave and guano is under current and continuous accumulation (Bento et al., 2011). Guano deposits are well preserved in the caves, without evidence of post-depositional reworking.

3. Materials and methods

This research explores a wide variety of materials such as speleothems, clastic sediments, soil, limestone bedrock and guano deposits from the same region. The chronology is based on U/Th in speleothems, optically stimulated luminescence in clastic sediments and radiocarbon dating in the guano deposits. All the methods and related applications are described below.

3.1. Speleothems

We have studied five speleothem samples from Chapada do Apodi: TRA7 from Trapiá Cave (27 cm deep), RN4 (105 cm deep) and RN1 (75 cm deep) from Rainha Cave, and ALE-1 (54.5 cm deep) and Abissal (21 cm deep), both from Abissal Cave (Figs. 1, 2 and Figs. S1-S3).

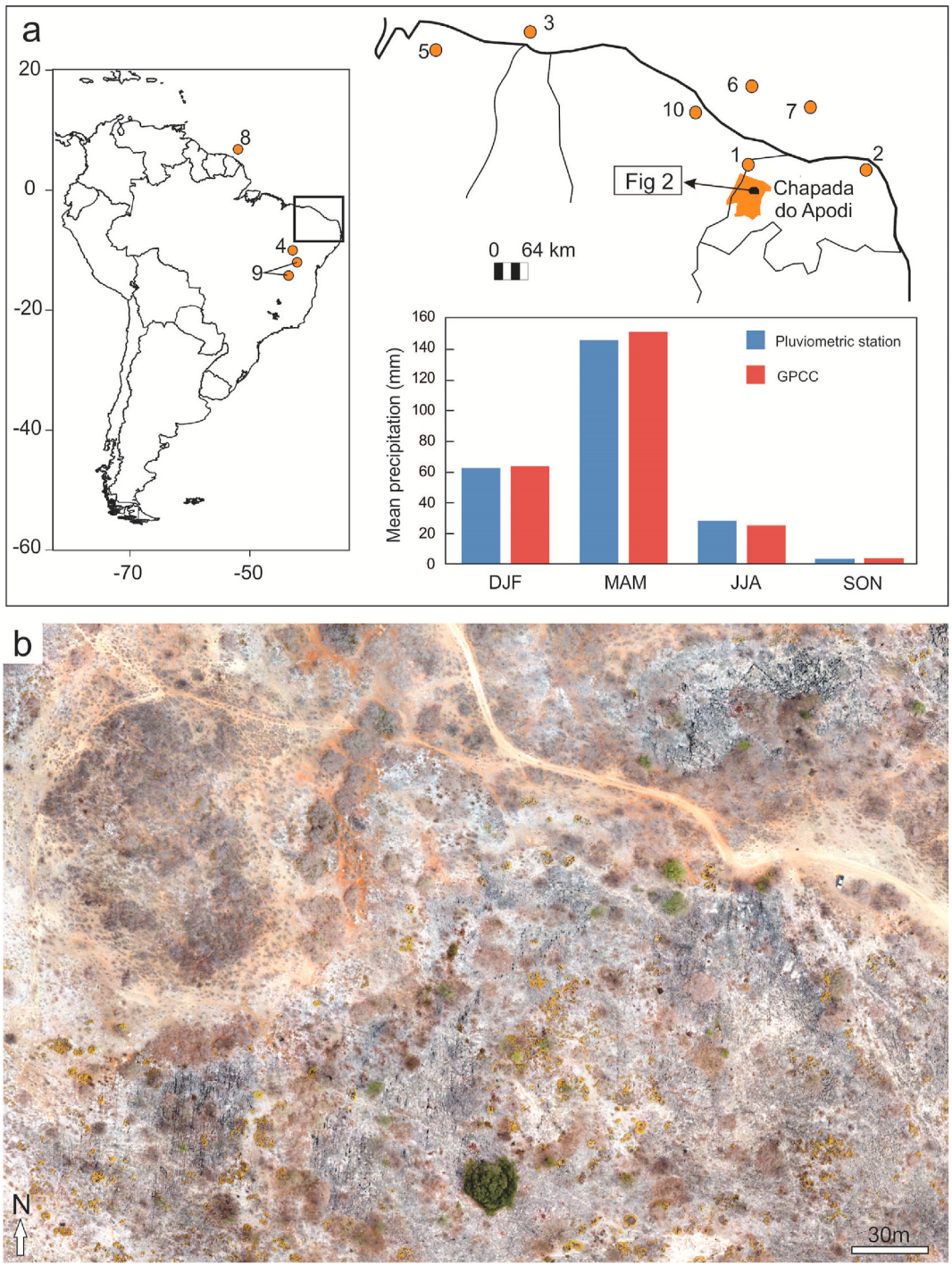

Fig. 1. Location of the study area in the context of previous paleo-environmental studies in Northeastern Brazil. a) NEB region, with Chapada do Apodi indicated by the orange area. Sites: 1 - Furna Nova Cave (Cruz et al., 2009), 2 - Boqueirão Lake (Utida et al., 2019), 3 - GeoB16202-2 (Mulitza et al., 2017), 4 - Icatú peat-bog (De Oliveira et al., 1999), 5 - Caçó Lake (Ledru et al., 2002, 2006), 6 - GeoB3104-1/3912−2 (Jennerjahn et al., 2004), 7 - GeoB3910-2 (Dupont et al., 2010), 8 - GeoB16224-1 (Zhang et al., 2017), 9 - Caves (Strikis et al., 2015, 2018), 10 - Serra de Maranguape (Montade et al., 2014). Mean pecipitation from Felipe Guerra, at Chapada do Apodi, for December, January and February (DJF), March, April and May (MAM), June, July and August (JJA), September, October and November (SON). Data from pluviometric station Pedra das Abelhas in Felipe Guerra municipality from Dec. 1910 to Nov. 2019 (# 537,008, 5.59S, 37.68W). The years 1931–1934 and 1942 were not registered (ANA – Agência Nacional de Águas). GPCC precipitation data for a grid of 1° (6S to 5S, 38 to 37W), from 1891 to 2016 (Ziese et al., 2018). Details are shown in Fig. 2 b) Drone image of the area around the Urubu Cave showing the reddish/yellowish relict soil areas in contrast with the typical grey color of the limestone outcrops of karst pavements. (For interpretation of the references to color in this figure legend, the reader is referred to the Web version of this article.)

The speleothems RN4, RN1, ALE-1, Abissal and FN1 (Furna Nova Cave, Fig. 1a, record # 1) were previously studied by Cruz et al. (2009) in a paleoclimate reconstruction based only on oxygen isotopic data (Table 1). Except RN1, these speleothems are deposited in the speleothem collection of the Geoscience Institute, University of São Paulo.

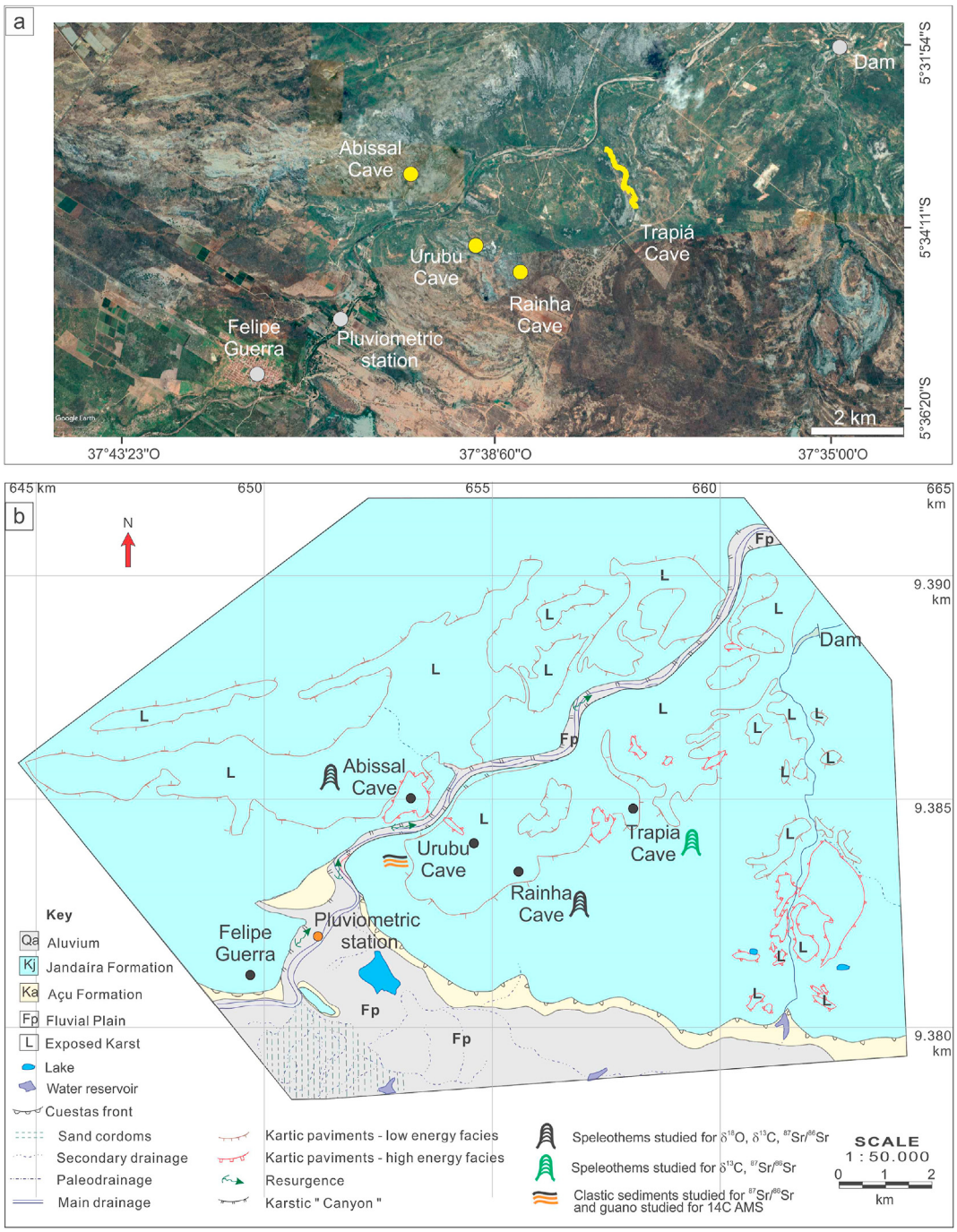

Fig. 2. Karst area located in Chapada do Apodi. a) Google Earth image depicting the karst pavement (light grey areas) and soil cover (brownish surface areas). Image data: Google Earth, Digital Globe 2019/CNES/Airbus 2019 (www.earth.google.com, [October 24, 2018]). b) Geological map of region portraying karst morphological features in the areas with exposed carbonate bedrock of Jandaíra Formation (the karst pavements) (modified from Cruz Júnior, 1996). The studied caves and pluviometric station of Pedra das Abelhas are located in both satellite image and geological map.

3.2. Carbonate bedrock sampling

Samples of carbonate bedrock were collected inside of Urubu Cave (two samples) and in the Lajedo Soledade, a nearby karst pavement (two samples) within the Apodi Group (5°35′40″S; 37°49′40″W). They were analyzed for carbon, oxygen, and strontium isotopes in order to compare with speleothem and clastic sediment data.

3.3. Clastic sediment sampling

Clastic sediment samples were collected in the first chamber of the Urubu Cave as indicated in section A of Fig. 3b. Samples for grain size analysis were collected at depths of 313 cm (B6A), 330 cm (B6B), 350 cm (B6C), and 445 cm (B6D). Samples for Optically Stimulated Luminescence (OSL) dating were retrieved using opaque PVC tubes at 350 cm (B6C) and 445 cm (B6D) depths. Charcoal fragments (cave-1-85) were collected at 345 cm depth for

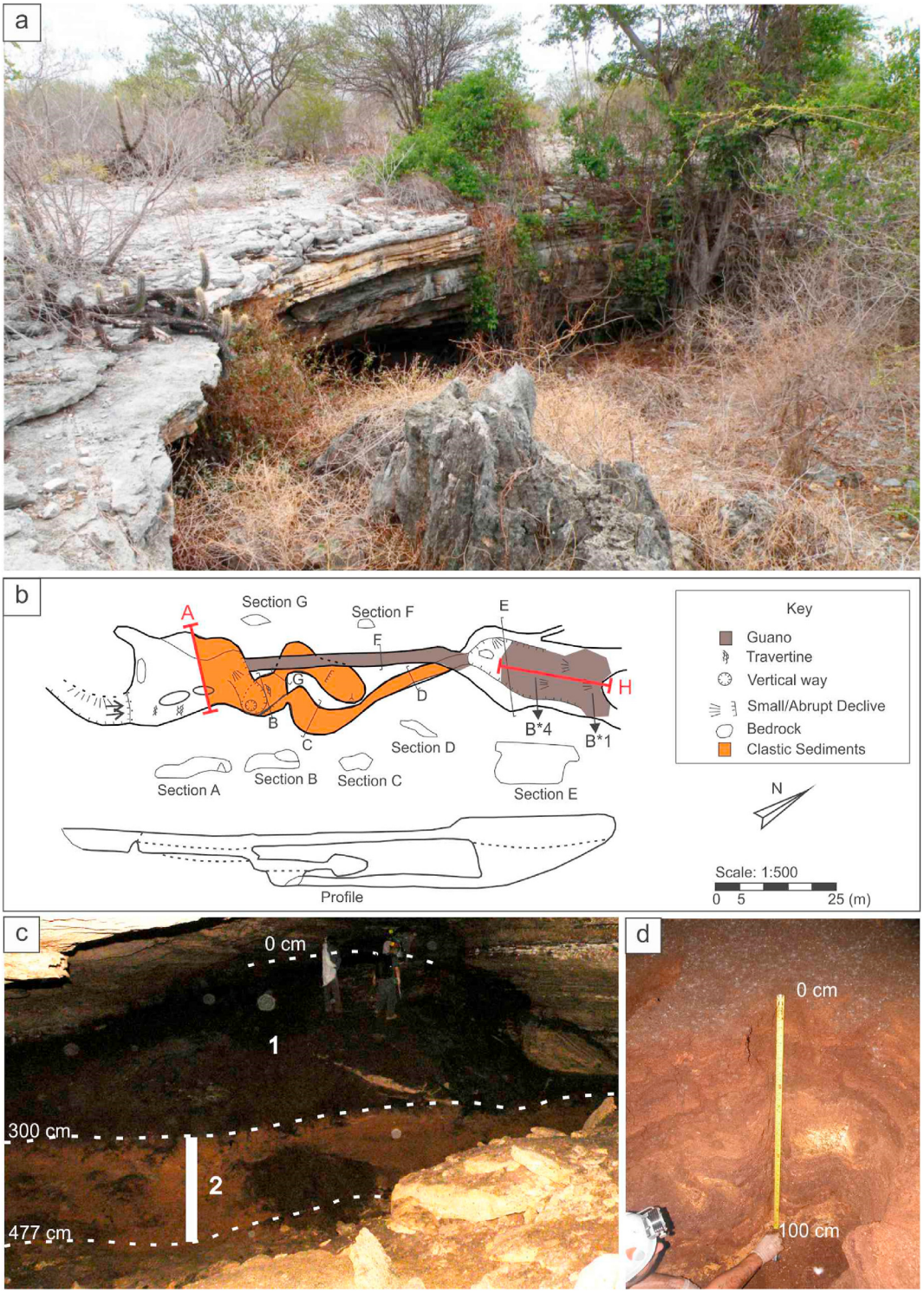

Fig. 3. a) Urubu Cave entrance. b) Urubu Cave map (Modified from Bento et al., 2011) with indication of sampling profiles (B*1 and B*4). c) Layer of clastic sediments (2) and guano deposits (1). White bar indicates where the clastic sediment samples were collected. d) Guano profile B1 in the upper-level gallery.

radiocarbon dating. Samples of residual soil were collected just above the entrance of the Urubu Cave for isotopic analysis.

3.4. Bat guano deposit

Samples of bat guano were collected in the second chamber of Urubu Cave for radiocarbon dating to reconstruct the chronology of accumulation. Five trenches of around 1 m × 1 m were excavated across the deposit until reaching the carbonate bedrock, probably representing fragments fallen from the ceiling (Section h in Fig. 3b, d). This same procedure was applied in the five guano profiles, named B1, B2, B3, B4 and B5 trenches and with depths of 100, 112, 56, 150 and 100 cm, respectively.

The five profiles were sampled from top to base with an

Table 1
Speleothem mineralogical composition according to the age and depth from the surface. * age estimated according to the age model.

Speleothem	Size	Age interval (BP)		Depth from the top (mm)	Age (BP)	Calcite (wt %)	Aragonite (wt %)
	(mm)	Min	Max				
TRA7	270	20	5,500	33	130	100.0	0.0
				82	360	100.0	0.0
				191	2,140	1.0	99.0
				248	4,530	12.1	87.1
FN1	200	0	3,670	11	440	14.8	85.2
				64	1,270	9.4	90.6
				102	1,610	100.0	0.0
				166	2,540	5.5	94.5
RN4	1,200	4,400	17,220	70	5,310	100.0	0.0
				260	7,710	100.0	0.0
				775	16,480	100.0	0.0
Ale1	510	15,120	17,260	16	15,180	100.0	0.0
				138	15,690	100.0	0.0
				295	16,350	100.0	0.0
				483	17,140	100.0	0.0
Abissal	210	24,220	25,750	166	21,494*	100.0	0.0
				180	23,547*	100.0	0.0

increment of 2 cm from the top to their base in order to avoid contamination from younger levels and collapse of the trench walls.

3.5. Chronology

3.5.1. U/Th dating

Twenty-two new U–Th ages were obtained for the TRA7 speleothem from Trapiá cave (Table S1). Each sample of ca. 150 mg was analyzed at the Minnesota Isotope Laboratory (University of Minnesota, USA) and at the Xi'an Jiaotong University (China), using a multi-collector inductively coupled plasma-mass spectrometry (MC-ICP-MS) technique, according to Cheng et al. (2013b). The speleothem age models were based on a linear regression between each age tie point and constructed using the COPRA model (Breitenbach et al., 2012) considering 2.000 Monte Carlo simulations and a 95% age confidence interval. U/Th data and age models of speleothems RN1, RN4, ALE1 and Abissal were obtained by Cruz et al. (2009). All U/Th age results are expressed in years (yrs) BP (1950).

3.5.2. Optically stimulated luminescence (OSL) dating

Samples at 350 and 445 cm depth were collected from profiles across clastic sediment deposits (Fig. 3b and c) for OSL dating. Sample preparation for luminescence measurements followed standard procedures (Aitken, 1998) to isolate quartz concentrates in the 120–150 μm grain size. Luminescence measurements were carried out in quartz aliquots using an automated Risø DA-20 TL/OSL reader equipped with a built-in $^{90}Sr/^{90}Y$ beta radiation source (dose rate of 0.088 Gy/s for cups), blue and infrared LEDs for light stimulation and Hoya U-340 filter for light detection in the ultraviolet band. Luminescence measurements were performed at the Federal University of São Paulo. Equivalent doses were determined using the single aliquot regenerative-dose (SAR) protocol (Wintle and Murray, 2006), with preheat of 200 °C (10s) and cutheat at 160 °C. Only aliquots with a recycling ratio within the 0.90–1.10 range, recuperation less than 5% and negligible infrared signal ensuring the absence of feldspar contamination were considered for equivalent dose calculation using the Central Age Model (Galbraith et al., 1999). A dose recovery test was performed with eight aliquots of sample B6C using a preheat temperature of 200 °C and given dose of 8.8 Gy. The calculated-to-given dose ratio was 0.97 ± 0.1, ensuring that the sample has quartz grains suitable to recover equivalent doses under laboratory conditions. For dose rate calculation, bulk samples were dried and packed in sealed plastic containers for gamma ray spectrometry. Radiation dose rates were obtained through concentrations of U, Th and K measured in a high-resolution gamma ray spectrometry system equipped with a HPGe detector with 55% relative efficiency, 2.1. keV energy resolution and encased in an ultralow background shield. The contribution of cosmic radiation to the dose rate was calculated based on the samples' latitude, longitude, elevation, and depth below surface, as outlined by the model presented in Prescott and Stephan (1982). Sample preparation for OSL measurements and gamma ray spectrometry were carried out at the Luminescence and Gamma Spectrometry Laboratory (LEGaL). All OSL age results were calculated in years ago relatively to the year of analysis (2015) and also presented in years (yrs) BP (1950).

3.5.3. Radiocarbon dating

The humin fraction of six guano samples from the B1, B2, B3 and B5 profiles (Table S2) were analyzed for 14C dating. They were extracted according to Pessenda et al. (1996). Samples were dried at 60 °C and all plant or insect fragments discarded by handpicking and after flotation in HCl 0.01M. The samples were chemically prepared by using the following procedures: 1) treatment with HCl 0.5M at 70–80C for 4h and washed with distilled water until the pH reached 3–4; 2) reaction with pyrophosphate-sodium hydroxide 0.10M for ca. 36h and washed with distilled water until pH reached 3–4; 3) hydrolisation with 3M HCl at 100 °C for 12h, washed with distilled water until pH reached 3–4; and 4) dried at 40 °C for 48h. Samples were analyzed following the standard procedure for liquid scintillation counting (Pessenda and Camargo, 1991) at the 14C Laboratory of the Center for Nuclear Energy in Agriculture (CENA), Piracicaba, São Paulo, Brazil.

The other six and eight guano samples obtained from the B1 and B4 profiles, respectively, and one charcoal sample (cave-1-85) collected in the sedimentary deposit (Fig. 3b and c, Table S2) at 345 cm were selected for AMS 14C dating. The standard procedure ABA (acid-base-acid) pretreatment was used for AMS 14C dating the guano samples. All samples were treated in hot 2M HCl acid for 1 h and rinsed to neutrality using DI-water (Deionized water); then socked in 0.125 M NaOH for an hour and rinsed to neutrality using DI-water; then socked in 2M HCl for 30 min and rinsed to pH 6 using DI-water. Samples were dried in oven overnight at 70 °C. About 2 mg of material from unknown samples and background and working standard wood samples were placed into preheated quartz tubes for sealed quartz tube combustion at 800 °C with 0.1g Cu, 0.5 g CuO granules and a few grains of Ag foil. Quartz tubes were

preheated at 800 °C for 2 h, and CuO granules were preheated at 800 °C one day before usage. The Cu grains and Ag foils were reduced using hydrogen gas under vacuum at 800 °C. The combustion was programmed for 2 h at 800 °C. Then samples were cooled from 800 °C to 600 °C for 6 h to allow Cu to reduce the NxO to nitrogen gas. The purified CO_2 was then collected cryogenically for AMS 14C analysis. Purified CO_2 was submitted to the Keck Carbon Cycle AMS Laboratory of the University of California-Irvine for AMS 14C analysis using a hydrogen-iron reduction method. A split of purified CO_2 was also analyzed for $\delta^{13}C$ values using the in-house Finnegan 252 IRMS (isotope ratio mass spectrometer) with a dual inlet device.

All radiocarbon ages are reported as years (yrs) BP (1950) and normalized for $\delta^{13}C$ of −25‰ VPDB (Stuiver and Polach, 1977). All 14C ages were calibrated according to the SHcal13 model curve (Hogg et al., 2013) and age models were developed at CLAM using the simple linear regression between each age tie point with a 95% confidence interval (Blaauw, 2010) and considering 2013 CE the age at the top, corresponding to the year of sampling and reported as cal yrs BP.

3.6. Stable isotopes analyses

3.6.1. Carbon isotopes in speleothems and bedrock

For each stable carbon isotope measurement, around 200 μg of powder was drilled consecutively from the sample and analyzed with an on-line system GasBench interfaced to a Finnigan Delta XL ratio mass spectrometer at the University of Massachusetts for RN1, RN4, ALE-1, and Abissal speleothems. Aliquots from the TRA7 speleothem and from the carbonate bed rock were analyzed by a GasBench interfaced to a Finnigan Delta V Advantage at the University of São Paulo. Stable carbon isotope ratios are represented as $\delta^{13}C$ and referred as permill deviation from the VPDB standard, with a precision of 0.1 permill.

Speleothem samples TRA7 and ALE-1 were sampled with 0.3 and 5 mm increments, which correspond to a resolution of 6.5 and 4 years, respectively. Speleothems RN1 and RN4 were sampled in 2 mm increments, while the sample Abissal was sampled at 0.4 mm intervals, which correspond to a minimum and maximum resolution of 2 and 77 years, respectively. The entire carbon isotope record sums up to 2,654 measurements from the speleothems TRA7, ALE-1, RN1, RN4 and Abissal, with 852, 99, 448, 517 and 89 measurements, respectively.

Two samples of carbonate host rock were collected inside of Urubu Cave. In order to have a more regional isotopic signal, we also collected two samples of carbonate bedrock from Lajedo Soledade, a karst pavement located in 20 km distance from the cave. All bedrock samples were analyzed in triplicates for carbon and oxygen isotopes.

3.6.2. Strontium isotopes – $^{87}Sr/^{86}Sr$

The Sr-isotope ratio analyses were performed at the Geochronology Laboratory of the University of Brasília, Brazil. Aliquots of 50 mg of carbonate powder were reacted with 3 ml of cold dilute HCl for 24 h. The solution was evaporated and the residue was taken in 2.5 N HCl. Sr was separated using a conventional ion-exchange technique. The Sr-isotope ratios were measured using a thermal ionization Finnigan MAT-262 mass spectrometer. The 2σ uncertainty on the measured $^{87}Sr/^{86}Sr$ ratios was below 0.2% and the value obtained for the ND-987 standard was 0.71024 ± 0.00004.

The strontium record is composed of 67 samples from three speleothems, which includes 14 samples from TRA7 (each ~20 mm), 17 samples from Abissal (each ~30 mm), and 36 samples from RN4 (each ~30 mm). We have also obtained Sr isotope ratios from two bedrock samples and one soil sample from the Urubu Cave, and from three samples of rock carbonate from the Lajedo Soledade site.

The bedrock and soil samples collected above the cave were used as end-member values for the strontium isotope ratios measured in the speleothems. The amount of bedrock strontium ($^{87}Sr/^{86}Sr_{bedrock}$) (BC) and soil strontium ($^{87}Sr/^{86}Sr_{soil}$) contribution to the speleothem signal ($^{87}Sr/^{86}Sr_{speleo}$) was calculated using the equation (Miller et al., 1993; Zhu et al., 2011):

$$BC = \left[\left(^{87}Sr/^{86}Sr_{speleo} - ^{87}Sr/^{86}Sr_{soil}\right) \Big/ \times \left(^{87}Sr/^{86}Sr_{bedrock} - ^{87}Sr/^{86}Sr_{soil}\right)\right] \times 100 \quad \text{(A1)}$$

3.7. Mineralogical analysis

The speleothem mineralogy was identified in layers with different textural characteristics, for instance in layers formed by crystals with mosaic and columnar fabrics and also by interbedded needle-like crystals. The mineralogical composition was determined in samples with approximately 20 mg by X-ray powder diffraction in a Bruker D8 diffractometer (Cu Ka, 40 kV, 40 mA, step 0.02°, 153 s/step, scanning from 3 to 105° 2q) at the NAP Geoanalítica Laboratory of the University of São Paulo. Qualitative analysis and Rietveld refinement were made with the Panalytical High Score 3.0 software and the Crystallographic Open Database (Gražulis et al., 2009), considering background (Sonneveld and Visser, 1975), weight fraction, cell parameters and sample displacement. Crystallographic data for the mineral phases were taken from Pokroy et al. (1989) for aragonite and from Paquette and Reeder (1990) for calcite. Results are presented in weight proportion (wt %).

3.8. Grain size measurements

Grain size analyses of samples at 313 cm (B6A), 330 cm (B6B), 350 cm (B6C) and 445 cm (B6D) depths in the clastic sediment deposits of Urubu Cave were carried out at the Sedimentology Laboratory of the Institute of Geosciences of the University of São Paulo. Grain size analyses were performed with a Malvern Mastersizer 2000 laser diffraction granulometer coupled with a Hydro 2000MU attachment and built-in ultrasound device. Results were tabulated in 1-phi interval classes and classified according to Wentworth (1922).

3.9. Archaeological data

A dataset of 267 archaeological radiocarbon dates originating from human activity were compiled in order to evaluate the relationship between demographic dynamics of the region and the climate changes during the Holocene defined in this study (Table S6).

4. Results

4.1. Speleothem description

The composite speleothem data from NEB extends back to 25,700 yrs BP with speleothems RN4, Abissal and Ale-1, all dated by Cruz et al. (2009). Except for the period from 15,100 to 13,200 yrs BP, the combination of these stalagmites provides a continuous isotopic record from 25,700 to 4,100 yrs BP (Table 1) with an average resolution of 25 yrs.

The TRA7 speleothem covers part of the last 5,000 yrs. It shows a hiatus between 4,100 and 2,250 yrs BP. The speleothem deposition is apparently continuous in the last ~2,250 yrs BP (Fig. 4, Fig. S1 and Fig. S4).

The speleothems older than 5,000 yrs used in this study are exclusively formed by calcite crystals with mosaic and columnar fabrics (Table 1, Figs. S2-S3). This is the case for speleothems RN1, RN4, Ale and Abissal. In comparison, the speleothem FN1 has a weight proportion of aragonite greater than 85%, except for the interval from 95 to 125 cm, between 1,280 and 1,520 yrs BP, when it is composed of 100% calcite (Fig. S3). The TRA7 speleothem is composed of aragonite from 173 to 265 cm, which corresponds to the period between 1,820 and 4,950 yrs BP. In contrasts, the first 82 cm of TRA7 that comprise the last 360 years of speleothem growth, it is only composed of calcite (Table 1 and Fig. S1).

4.2. Speleothems and host-rock

4.2.1. Stable carbon isotopes

The speleothem $\delta^{13}C$ and $^{87}Sr/^{86}Sr$ isotopic record for the time interval from 25,900 yrs BP to the last century is presented in Fig. 4 and Table 1. The dataset of $\delta^{13}C$ and $\delta^{18}O$ from studied speleothems is known as Rio Grande do Norte record, hereafter RN record, as named in Cruz et al. (2009).

The $\delta^{13}C$ record from the RN4 and RN1 speleothems varies between −13 and 1.5‰; hence it is characterized by a large amplitude of 14.5‰ (Fig. 4a). From 25,700 to 18,500 yrs BP $\delta^{13}C$ values drop from −7 to −9.5‰. Between 18,500 BP and 15,000 yrs BP there is an enhanced variability of the $\delta^{13}C$ values (varying between −5.2 and −13‰). The higher values (−5.2‰) in this interval occur around 16,700 yrs BP. Between 15,000 and 13,000 yrs BP there is a hiatus in precipitation that is followed by an interval with the lowest $\delta^{13}C$ values (−12.8‰) of the record (13,000 to 5,000 yrs BP). Between 5,000 yrs BP and the most recent portion of the RN1 and RN4 records, there is an abrupt enrichment of $\delta^{13}C$ from −10‰ to +1.3‰ in both speleothems (Fig. 4a). Consistent with the speleothems from Rainha cave, the speleothem TRA7 from Trapiá cave also shows enriched $\delta^{13}C$ values, reaching +1.03‰ for the interval between ~5,000 and 4,100 yrs BP (Fig. 4), followed by a hiatus from 4,100 to 2,250 yrs BP. After 2,250 yrs BP, $\delta^{13}C$ values are more depleted and vary between −7.3‰ and +0.0‰, reaching the most depleted values at the present. The highest $\delta^{13}C$ values observed in the dataset from 5,000 to 4,100 yrs BP are within the range of $\delta^{13}C$ values for the Cretaceous carbonate bedrock, which varies between −1.35 and 0.92‰ for samples from the Urubu Cave and between 0.98 and 1.62‰ for samples from the Lajedo Soledade (Fig. 4a and Table S3).

4.2.2. Strontium isotopes

$^{87}Sr/^{86}Sr$ values of the ALE-1, RN4, and TRA7 stalagmites cover the time interval from 17,200 yrs BP to the last century (Fig. 4e). The values range from 0.7085 to 0.7115, with an average value of 0.7098. From 17,200 to 10,000 yrs BP, $^{87}Sr/^{86}Sr$ values have an average value of 0.7094, interrupted by a hiatus from 15,100 to 13,200 yrs BP and 5,000 to 4,100 yrs BP. An abrupt increase in the $^{87}Sr/^{86}Sr$ values occurs from 9,200 to 4,100 yrs BP, with an average value of 0.7110, which corresponds to the maximum values recorded. Between 4,600 and 4,300 yrs BP, there is an abrupt transition to lower $^{87}Sr/^{86}Sr$ values ranging from 0.7110 to 0.7086 (Fig. 4e), followed by the hiatus in TRA7. From 2,200 yrs BP to the present, $^{87}Sr/^{86}Sr$ values gradually become more enriched, up to 0,7100.

4.3. Sedimentary deposits of the Urubu Cave

4.3.1. Clastic sediments

The clastic sediment deposits of the Urubu Cave display different proportions of silt and sand. While the interval between 313 and 350 cm depth consists of 51–54% silt and 20% sand, the interval near the base of the profile (445 cm depth) consists mainly of medium and fine sand with minor percentages of silt and clay (Table S4).

Quartz grains found at 350 cm and 445 cm depth exhibited strong natural OSL signals dominated by the fast OSL component and equivalent doses of 13.0 ± 0.4 and 15.3 ± 0.5 Gy, respectively. Overdispersion values of equivalent dose distributions were 10 and 12%, pointing to well-bleached sediments without significant post-depositional mixing. Dose rates were 2.558 ± 0.166 and 2.107 ± 0.142 Gy/ka, resulting in OSL ages of 5,115 ± 364 yrs (5,050 yrs BP) and 7,415 ± 545 yrs (7350 yrs BP) at the depths of 350 and 445 cm, respectively (Figs. 4g, 5a). OSL dating results are shown in Table S2.

The AMS age on the charcoal found at 345 cm depth in the sediment profile equals 4,235 cal yrs BP (3,880 ± 20 ^{14}C yrs BP), being consistent with the OSL age at 350 cm depth (Figs. 4g, 5a).

$^{87}Sr/^{86}Sr$ results of these sediments from Urubu Cave vary between 0.7177 and 0.7223 with an average value of 0.7199 (Fig. 4f and Table S5). The lower value occurs at the base of the sequence (7,400 yrs), where a higher content of sand grains is observed (Table S4). The $^{87}Sr/^{86}Sr$ values reach their maximum at a depth of 350 cm (5,100 yrs) and decrease to around 0.7196 at the top of the sequence. These values are very similar to the ones measured in the soil samples collected above the cave, which are 0.7194 and 0.7219, respectively (Fig. 4f and Table S5).

4.3.2. Chronology of guano deposit

The bat guano chronology is based on nineteen AMS 14C dates distributed along five different profiles excavated in the upper-level gallery of Urubu Cave (Table S2). The guano deposit started accumulating at around 2,740 cal yrs BP and continues to the present time, considering the age of the deepest sample (B5-70) and the youngest age of the top guano sequence (B2-0), respectively (Fig. 4g, Table S2 and Fig. S5). The age models for B1 and B4 profiles show guano accumulation from 1770 to 96 cal yrs BP (Fig. S5). There is an interval of lower deposition extending from 835 to 295 cal yrs BP in B1 and from 1220 to 90 cal yrs BP in B4.

5. Discussion

5.1. Climatic and environmental reconstruction

The isotopic composition of rainfall in this sector of NEB is interpreted as primarily influenced by the amount of precipitation with a decrease (increase) in $\delta^{18}O$ and δD corresponding to enhanced (weakened) ITCZ rainfall on interannual and seasonal timescales forced by insolation (Fig. 1a, record # 2–3, 4b, 4h) (Cruz et al., 2009; Mulitza et al., 2017; Utida et al., 2019). Thus, speleothem $\delta^{18}O$ records at the study site can be used to reconstruct environmental changes that are associated with precipitation variability (Fig. 4b; Cruz et al., 2009).

According to different $^{87}Sr/^{86}Sr$ signatures obtained for bedrock and soil above the cave (Fig. 4e and f), they were considered the end-members for Sr speleothem contribution allowing interpretation of their sources (Fig. 4e and f). In our NEB karst area, the major strontium source for speleothems is the local bedrock, as attested by greater similarity with values measured in the speleothem (Fig. 4d). Another source of Sr is the soil above the cave, which has more radiogenic Sr isotope values. In the absence of sand dunes

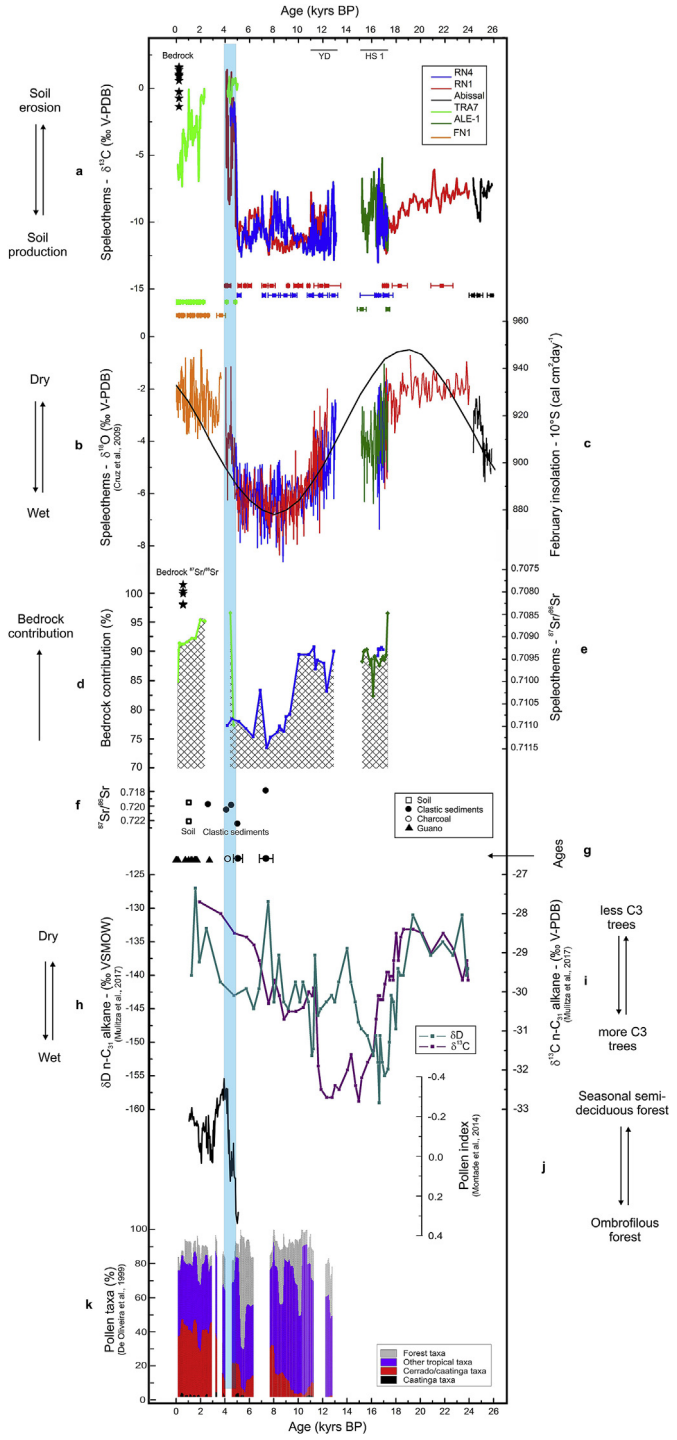

Fig. 4. Paleoclimate data from the RN record. a) $\delta^{13}C$ of speleothems and bedrock (asterisks) (this study). U/Th dates of RN1 and RN4 speleothems (blue and red dots) (Cruz et al., 2009). U/Th dates of TRA7 obtained in this study are marked with light green dots. b) $\delta^{18}O$ of Rainha cave (Cruz et al., 2009) and Trapiá speleothems (this study). c) Insolation at 10°S (Berger and Loutre, 1991). d) Calculated bedrock contribution in speleothems according to equation (eq. (A1)) based on $^{87}Sr/^{86}Sr$ of sediments and bedrock samples (stars). e) $^{87}Sr/^{86}Sr$ for NEB speleothems and bedrock (this study). f) $^{87}Sr/^{86}Sr$ for soil and clastic sediments of Urubu Cave. Bedrock and soil are the end-members for bedrock contribution. g) Chronological results: OSL for clastic sediments, AMS 14C calibrated ages for charcoal collected in clastic deposit and guano. h) δD and i) $\delta^{13}C$ for n-alkanes from GEOB16202-2 (Mulitza et al., 2017). j) Pollen index from Serra de Maranguape (Montade et al., 2014). k) Pollen taxa from Icatu River valley (De Oliveira et al., 1999). Blue shaded area indicates the transition period between 5,000 and 4,200 yrs BP. Younger Dryas (YD) and Heinrich Stadial 1 (HS1) defined by changes in speleothem $\delta^{18}O$ from Rainha cave (Cruz et al., 2009). (For interpretation of the references to color in this figure legend, the reader is referred to the Web version of this article.)

or eolian dust deposits in the area, we rule out a significant contribution of wind-transported sediments to strontium isotopes in the speleothems as observed in areas that are more directly influenced by dust transport from deserts (Ayalon et al., 1999).

There is a small variation in the $^{87}Sr/^{86}Sr$ values of bedrock carbonate samples collected in Urubu Cave and Lajedo de Soledade sites, with values near 0.7080 (Fig. 4e and Table S5). Our results are similar to $^{87}Sr/^{86}Sr$ values reported for Cretaceous carbonate rock samples from NEB (Bertotti et al., 2017) as well as to globally averaged Sr isotope ratios of marine carbonate rocks (Veizer, 1989; McArthur et al., 2001). Thus, we infer that the $^{87}Sr/^{86}Sr$ ratios of the speleothem are not controlled by differences in the bedrock Sr signal. Variability of the $^{87}Sr/^{86}Sr$ in NEB speleothems (Fig. 4e) results from variations in water residence time in the system and, consequently, the relative proportion of Sr derived from the bedrock and from the soil directly above the cave (e.g. Wortham et al., 2017; Novello et al., 2019; Ward et al., 2019). The proportion of these two main sources of Sr is closely related to changes in the precipitation amount (e.g. Ayalon et al., 1999; Zhou et al., 2009; Hori et al., 2013).

During periods of increased precipitation, water percolates faster throughout the karst system. Under such conditions, percolating water has a lower residence time and water-rock interaction is reduced, resulting in water with more radiogenic $^{87}Sr/^{86}Sr$ ratios and distinct from the bedrock values (Novello et al., 2019; Ward et al., 2019). The higher $^{87}Sr/^{86}Sr$ ratios observed during intervals with lower $\delta^{18}O$ values indicate that the precipitation amount is the main process controlling the Sr isotope signal of the RN speleothem (Fib. 4). For instance, the highest $^{87}Sr/^{86}Sr$ values occur during the period of maximum precipitation in the area, from 9,000 to about 5,000 yrs BP, which corresponds to a time when the water residence is reduced in the vadose karst aquifer, and therefore, the contribution of Sr from bedrock (low $^{87}Sr/^{86}Sr$ values) is minimal, while the source contribution is up to 30% from soil (Fig. 4d, according to equation (A1)). On the other hand, intermediate and low $^{87}Sr/^{86}Sr$ values are observed during the deglacial period at the transition to the Holocene (17,000 to 9,000 yrs BP), and during the Late Holocene (2,200 yrs BP to present). The intermediate values observed between 17,000 and 9,000 yrs BP can be explained by the large precipitation fluctuations that mark the transition from LGM to the deglaciation, as indicated by the $\delta^{18}O$ and speleothem hiatuses from 15,000 to 13,000 yrs BP at the time of the Bolling-Allerød dry event (Fig. 4). In contrast, the lowest $^{87}Sr/^{86}Sr$ values observed between 5,000 yrs BP and the present correspond to a period of reduced water infiltration and, hence, a longer water residence time in the vadose zone during prevailing dry climate conditions that characterize the Late Holocene in the region, which reflects a much reduced soil contribution of only 5–15% (Fig. 4d, according to equation (A1)). This notion of a dry period is reinforced by the absence of speleothem deposition between 4,000 and 3,600 yrs BP (Fig. 4). The predominance of aragonite from 4,500 to ~4,200 yrs BP in the TRA7 and FN1 speleothems also suggests carbonate precipitation under dryness for this period, as described in other regions (Cabrol and Coudray, 1982; Frisia et al., 2002; Fairchild et al., 2006).

The other possibility for high $^{87}Sr/^{86}Sr$ values from Early to Middle Holocene in NEB is the enhanced weathering in response to a wetter climate combined with reduced erosion rates, which would promote soil layer thickening above the cave. This scenario would result in a higher availability of radiogenic Sr in thicker soils above the cave (Fig. 4). High rates of soil accumulation could also explain the more negative $\delta^{13}C$ values of speleothems observed in the same period, which would have increased the contribution of more depleted carbon derived from organic material in the soil (Burns et al., 2002; Genty et al., 2003; Cruz et al., 2006; Denniston et al., 2017; Jones et al., 2018). This assumption is supported by the

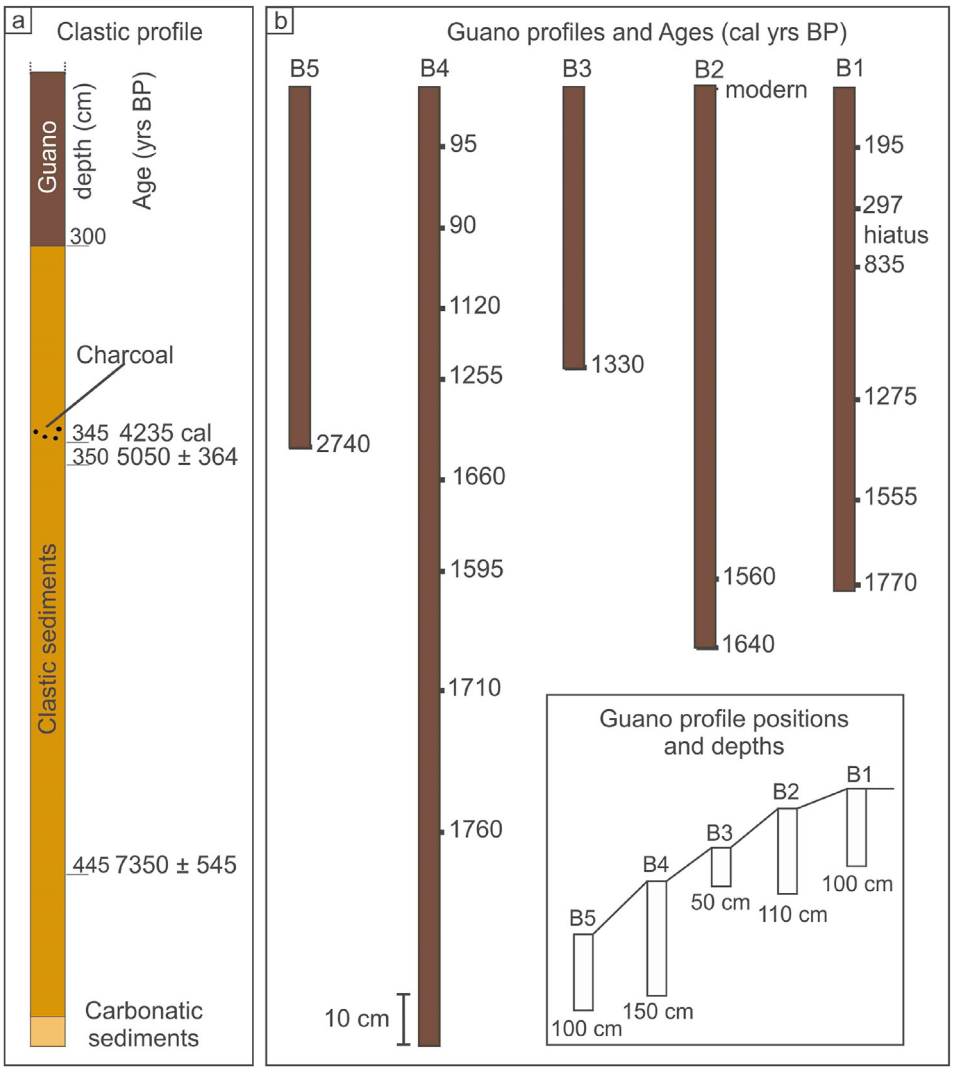

Fig. 5. Urubu Cave sediment profiles. a) Clastic sediment profile with OSL and AMS 14C calibrated dates according to depositional depth. The clastic profile is located in the trench of section A (Fig. 3b and c). b) 14C calibrated dates according to depositional depth for guano profiles B1 to B5. Profiles are located in the cross-section H of the cave map (Fig. 3b, d-e).

presence of very negative $\delta^{13}C$ in bulk organic matter (OM) of soils, which varies from −24 to −32‰ in the areas covered by caatinga dry forest in NEB (Pessenda et al., 2010). However, the $\delta^{13}C$ of speleothems could not be used to investigate changes of the vegetation type, as the isotopic values in the OM of these soils show a similar range to the ones covered by rainforest in coastal humid areas in Brazil (e.g. Calegari et al., 2017; Buso Junior et al., 2019).

Conversely, the abrupt change in both $\delta^{13}C$ and $^{87}Sr/^{86}Sr$ ratios of the speleothems from Middle to Late Holocene suggests that soil erosion processes are dominant during the last four millennia because of the prevailing dry climate (Fig. 4). Drier climate increases soil erosion rates due to development of a less dense vegetation cover, exposing soils from past wetter periods to erosion during rainfall events, similar to the interpretation for central Texas based on Sr results (Cooke et al., 2009). Indeed, the high values of speleothem $\delta^{13}C$ during this period are consistent with the isotope range of carbonate bedrock (−1.35 to +1.62‰), indicating that soil was almost completed washed away from the surface. Furthermore, the low $^{87}Sr/^{86}Sr$ values are very close to the Cretaceous carbonate rock signal, which contributes with 95% of the strontium isotope composition of speleothems.

Internal fractionating mechanisms that are effective in the vadose zone and during the speleothem deposition in the cave, such as prior calcite precipitation and the rate of CO_2 degassing (Fairchild et al., 2000; McDermott, 2004; Johnson et al., 2006) could at least in part explain the carbon isotope fluctuations in the RN record. However, they cannot produce such a sudden shift of 12–13‰ as occurred between 4,800 and 4,200 yrs BP (Fig. 4a). This shift is highly anomalous considering the much smaller amplitude of ~5‰ observed from 13,000 to 5,000 yrs BP. Furthermore, the $^{87}Sr/^{86}Sr$ variation is independent of any fractionating processes and relies almost exclusively on the contribution from the bedrock source during the Late Holocene.

By considering that the cave drainages are non-active in the area at present, the clastic sediment deposits in the Urubu Cave point to a past wetter climate. The lack of primary structures and the predominance of muddy sediments (Table S4) point to deposition of water-laid sediments during a wetter period (Fairchild and Baker, 2012). Thus, we interpreted the clastic deposit in Urubu Cave as a proxy for hydrological changes in the region.

Clastic sediments in cave drainages such as in Trapiá cave and the Rainha-Urubu cave system originate in the carbonate rock area with no influence from Cretaceous sandstones (Fig. 2). This implies that the siliciclastic sediments accumulating in the cave deposits

would derive from terrigenous components disseminated within the carbonate rocks and concentrated by weathering in soils, as confirmed by the close similarity in $^{87}Sr/^{86}Sr$ values between soil and clastic sediments.

The OSL and ^{14}C ages from the clastic deposits indicate that the cave drainage was active between 8,000 and 4,200 yrs BP (Fig. 5). These results suggest that the relatively wet climate was responsible for a fast soil turnover during this period due to an enhancement in both soil accumulation and erosion above the cave, according to $\delta^{13}C$ and $^{87}Sr/^{86}Sr$ speleothem results. In addition, the upward change in grain size, characterized by an increasing proportion of silt and clay (Table S4) in the cave sediment sequence, suggests a decrease in flowing water and deposition under lake-like conditions due to fluvial channel impoundment. On the other hand, the lack of younger clastic deposits might be attributed to weaker underground streamflow due to a drier climate, which also lead to decreased soil availability at the surface.

The presence of thick bat guano deposits in the Urubu Cave reflects the lack of major fluvial activity in the cave at least since 2,700 cal yrs BP, according to guano ages and the age model (Table S2 and Fig. S5). The absence of active fluvial channels since this period is attributed to the continuous and well-preserved guano sequence, which has high solubility to percolating water. These organic deposits started accumulating about 2,700 cal yrs ago, during a period of increased aridity in the region, as indicated by high $\delta^{18}O$ values of speleothems. The lack of water flow is evident during the entire interval of guano deposition as indicated by the consistent distribution of the twenty ^{14}C dates, pointing to continuous deposition of guano.

5.2. Implications of RN multiproxy speleothem data for paleoenviromental reconstruction in NEB

Although the speleothem $\delta^{13}C$ record is not suitable to distinguish changes in the type of vegetation, the data set that comprises the RN record can be associated with vegetation density and changes from more humid-to dry-adapted forests based on pollen, charcoal and organic geochemistry archives (Fig. 1, record # 3–7) (De Oliveira et al., 1999; Ledru et al., 2002; Jennerjahn et al., 2004; Jaeschke et al., 2007; Dupont et al., 2010; Mulitza et al., 2017; Mota and Scheel-Ybert, 2019).

The data from the RN cave site contributes new evidence to the discussion of paleoenvironmental changes in NEB; in particular, during periods of abrupt shifts in climate. For instance, the transition from the LGM to the HS1 period is marked by an abrupt change from drier to wetter climate in NEB at about 17,500 yrs BP (Cruz et al., 2009). This event also coincides with a broad expansion of humid forests over a large latitudinal range and from mountainous areas down to the plains, as indicated by pollen in several records across Brazil (Pinaya et al., 2019). This expansion of plant species that are typical of wet climates in NEB might have been sustained by the spread of pioneer-species towards a dense rain forest rich in *Podocarpus*, according to the pollen evidence from Caçó Lake (Ledru et al., 2006; Pinaya et al., 2019) (Fig. 1, record # 5).

These shifts in vegetation are also coincident with wetter climate as depicted by very low $\delta^{18}O$ values in the RN record and other speleothem records from NEB (Fig. 1, record # 9) (Strikis et al., 2015, 2018). The same interpretation is valid for the δD records from leaf wax (Fig. 1, record # 3) (Mulitza et al., 2017) and Ti/Ca and Fe/Ca from marine records offshore NEB (Fig. 1 record # 6 and 8) (Arz et al., 1999; Jennerjahn et al., 2004; Zhang et al., 2017).

Despite the more depleted carbon isotopes in speleothems and marine sediment records being commonly associated with C3 vegetation that prefers humid climate conditions, the RN record displays an increase in $\delta^{13}C$ at the beginning of the HS1 event (Fig. 4 a). The start of HS1 is characterized by a peak in $\delta^{13}C$ values at~16,800 yrs BP in the RN record, which is likely associated with soil erosion, resulting from increased water runoff during the wet interval. Similarly, Mulitza et al. (2017) interpreted the increase in Fe/Ca ratios in the marine core off the Northeast coast as enhanced terrigenous input during HS1, related to removal of soil due to erosion in the catchment (Fig. 1a, record # 3, and Fig. 4h and i).

The soil erosion at the beginning of HS1 might be attributed to the sparse vegetation that made the soils more susceptible to widespread erosion. Just after 16,800 yrs BP, the more negative $\delta^{13}C$ values in the speleothems suggest a higher contribution from more depleted carbon from soils, possibly connected to the development of denser vegetation (Fig. 4 a-b). The response of vegetation to the changes in precipitation is interpreted as being asynchronous in the region during HS1 (Fig. 1, record # 6; Jennerjhan et al., 2004; Dupont et al., 2010).

In the case of marine sediments, the reduced variability in the $\delta^{13}C$ of n-alkane long chains related to arboreal vegetation is not exactly following the hydrological variations interpreted from the δD record in the same core (Mulitza et al., 2017, Fig. 4h and i). This is probably because the proportion of C4 to C3 plants does not change significantly, despite vegetation changes recorded over the continent and NEB and other continental areas in Brazil (Behling et al., 2000; Ledru et al., 2006; Dupont et al., 2010; Pinaya et al., 2019). The humid period during HS1 is succeeded by a dry period associated with the Bolling-Allerod event, which is marked by a hiatus in the speleothem deposition in the region from 15,000 to 13,200 yrs BP.

The climate transition from the interval equivalent to the Younger Dryas (YD), between 13,200 and 11,000 yrs BP, and the Holocene, is marked by a long-term trend toward lower $\delta^{18}O$ and $\delta^{13}C$ values in the RN record, but variability during this period remains high (Fig. 4). These data, when combined with the strontium isotopes and the chronology of clastic sediment deposits, point out a long wet period that lasted six millennia until ~5,000 yrs BP. The wetter phase contributed to an expansion of taxa from rainforest in NEB in the Early Holocene, with presence of major pollen taxa such as *Cecropia*, *Ilex*, Melastomataceae and Myrtaceae (Fig. 1 record #4–5, Fig. 4-k) (De Oliveira et al., 1999; Ledru et al., 2006). During the most humid period in the Middle Holocene, the pollen record is characterized by tropical forest taxa, especially represented by *Mauritia* pollen (De Oliveira et al., 1999; Ledru et al., 2006) and arboreal taxa such as *Alchornea*, *Pterocarpus* and Urticaceae/Moraceae (De Oliveira et al., 1999). Some of the taxa are typical for the Brazilian Savanna vegetation (the Cerrado), which needs a significantly longer rainy season in comparison with the modern vegetation, the caatinga dry forest.

The wetter climate was interrupted by the establishment of drier conditions in the Late Holocene, particularly after the 4,200 yrs BP event. These results are in agreement with studies of vegetation dynamics that report the dominance of savanna (caatinga) in the same time interval when precipitation increased (decreased) in NEB in the Early to Middle (Late) Holocene (De Oliveira et al., 1999, Fig. 1, record # 4, Fig. 4k). There is a tendency towards progressively more arid conditions indicated by an increase in grasses (Gramineae = Poaceae) and sedge (Cyperaceae), and pollen of caatinga and cerrado taxa, e.g., *Byrsonima*, *Chamaesyce*, *Cuphea*, *Curatella*, *Mimosa* and *Ouratea* (Fig. 1, record # 4, Fig. 4-k) (De Oliveira et al., 1999). Between 4,600 and 2,900 yrs BP, there is also a discontinuity of pollen preservation in NEB, similar to the hiatus in speleothem deposition, also indicating a drier interval (Fig. 4k).

In addition, the marine record offshore NEB also suggests opening of forest during the Late Holocene, as inferred from the

increase in C4 grass species at the time when the caatinga forest retracted and a semi-arid climate was established in the region (Mulitza et al., 2017, Fig. 4i). This notion is supported by vegetation model simulations that show dominance of savanna in the Middle Holocene, while open shrubland, typical of caatinga dry forest, expanded in NEB during the last 4,000 yrs BP (Maksic et al., 2018).

The overall interpretation considering the different proxies and model simulations for the paleoclimate and paleoenvironmental conditions of the study area are summarized in Fig. 6. Our findings document striking environmental changes because of changes in the ITCZ rainfall throughout the Holocene in NEB. In particular, the predominance of savanna or Brazilian cerrado during the wettest period identified in the $\delta^{18}O$ of speleothems indicates a longer rainy season from 9,000 to 5,000 yrs BP (Figs. 4, 6a). The savanna requires rainfall that is well-distributed over 5–6 months; climatic conditions that are significantly different from modern climatology in which the ITCZ rainfall is mostly restricted to the austral autumn (March to May) (Ratter et al., 1997; Beuchle et al., 2015). A longer rainy season probably resulted from a more active ITCZ during the previous summer months, consistent with reduced mid-tropospheric subsidence in the region, driven by low summer insolation in the southern hemisphere during the Early to Middle Holocene, possible associated with a southward displacement of the ITCZ (Cruz et al., 2009).

In the Chapada do Apodi, more humid conditions and a less seasonal climate led to enhanced carbonate bedrock dissolution and thicker soil formation in the area of karst pavements during the Middle Holocene, as suggested by the carbon and strontium isotopes in the RN record (Fig. 6a). The chronology of clastic sediments confirmed that the cave drainages were active during this period. It is likely that the relatively dense vegetation aided in preventing the soils from being eroded entirely.

The interval from 5,000 to 4,200 yrs BP is marked by an abrupt transition of the environmental conditions (Fig. 4a–g). Our results indicate that the contribution of organic carbon from soil with depleted $\delta^{13}C$ and high $^{87}Sr/^{86}Sr$ strongly diminished in the $\delta^{13}C$ and $^{87}Sr/^{86}Sr$ speleothems, which suggests massive erosion of the soil mantle, thereby exposing the pavements in a large area

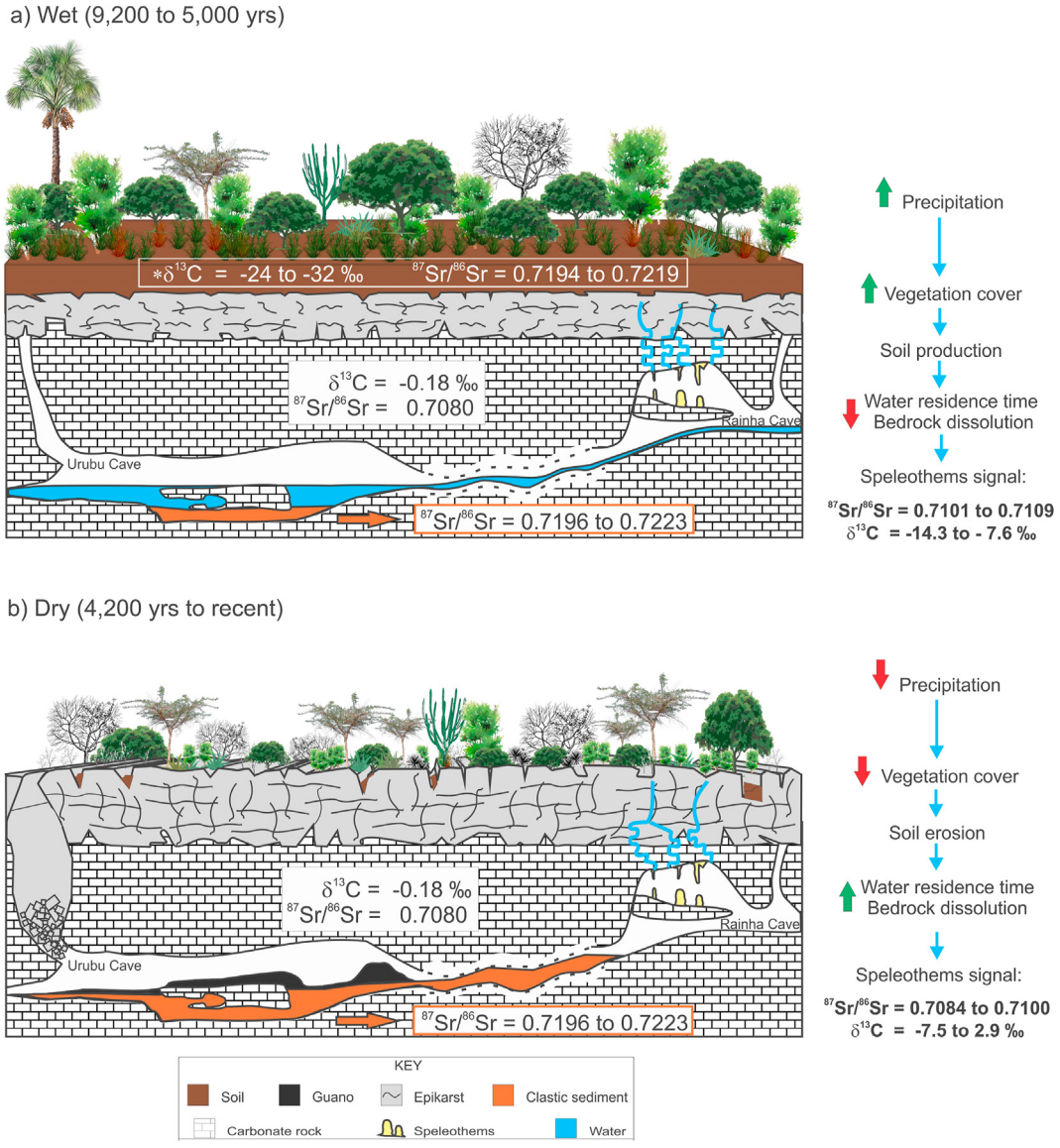

Fig. 6. Conceptual model for the environmental changes in the Rainha-Urubu cave system based on isotopic proxies: a) wet conditions observed from 9,200 to 5,000 yrs BP and b) dry conditions observed from 4,200 yrs BP to the present.

corresponding to approximately 67 square kilometers (Fig. 6b). This idea is reinforced by the end of clastic sediment deposition inside the Urubu Cave around 4,000 yrs BP (Figs. 3c and 4g), suggesting limited soil availability for erosion in the cave river watershed and above the cave. In addition, the undisturbed bat guano accumulation confirms that cave rivers were not active during the Late Holocene. Age differences among guano profiles and observed age inversions in B4 may be attributed to the guano slipping from the top of the deposit (Fig. 5 and S8).

The beginning of the Meghalayan Age was also marked by a sharp vegetation transition, as documented in pollen records from an adjacent site in NEB. At Serra do Maranguape (Fig. 1, record # 10), *Ficus* was the dominant taxon at the end of the Middle Holocene and abrupt declined after 4,790 cal yrs BP, recording the first vegetation change. The second vegetation change occurred after 4,275 yrs BP, when the main components of the forest declined. They were represented by the assemblage of Moraceae/Urticaceae-type and Myrtaceae that characterize the dense ombrophilous montane forest. At the same time, *Alchornea,* that represents tree species considered as early successional and heliophilous trees growing in forest gaps, increased considerably and just declined after 3,525 yrs BP (Montade et al., 2014). The fast increase of pollen from *Alchornea* contributed to a decline in the pollen index, interpreted as an increase in taxa more adapted to dry climates, in accordance with our speleothem isotope record pointing toward drier conditions after 4,200 yrs BP (Fig. 4-j). Hence, the establishment of sparser vegetation might have resulted in a soil mantle more susceptible to erosion processes by episodic rains. Depleted $\delta^{13}C$ and high $^{87}Sr/^{86}Sr$ indicate a return to more vegetated areas and increased soil production after 3,000 yrs BP. This is also observed in the pollen index (Fig. 4-j), represented by a gradual recovery of ombrophilous montane forest (Montade et al., 2014).

The main forcing mechanism, already described for the NEB region related to precipitation, is intimately correlated with orbital forcing (Cruz et al., 2009). The 4.2 ka event is positioned near the inflection point of this precessional curve, but there is no strong evidence that would point to orbital forcing as responsible for the event. Some authors attribute the triggering of the 4.2 ka event in some location in the Northern Hemisphere to the southward migration of the ITCZ (e.g. Mayewski et al., 2004; Zanchetta et al., 2016), but it is unlikely to be the cause of drier conditions in the region as an ITCZ movement to the south would increase precipitation over NEB.

5.3. Archaeological implications

Northeastern Brazil has a rich archaeological record, documenting the systematic and continuous human occupation of the region during the entire Holocene. The demographic dynamics of the region were evaluated for this period and compared with the paleoclimatic data of NEB. We compiled a dataset of 267 archaeological radiocarbon dates originating from human activity in the region (Table S6 and Fig. S6).

The overall pattern for NEB is similar to what was previously described for other regions of Brazil and South America (e.g. Araujo et al., 2005; Goldberg et al., 2016; Riris and Arroyo-Kalin, 2019) with a high frequency of radiocarbon dates during the Early and Late Holocene and a low frequency during the Middle Holocene.

Between ca. 12,500–8,000 yrs BP NEB was occupied by different groups composed of generalist foragers adapted to varying local environments. Stone tool (lithic) technology was diverse including uni- and bi-facial knapping that produced both expedited and curated assemblages (Martin, 2013). Although bifacial projectile points are known for the region, the defining artifacts for this time period in NEB are uni-facial limaces produced over long flakes (a.k.a. plane-convex or unifaces) (Lourdeau, 2015). These artifacts define the Itaparica Tradition and are found over an area stretching ca. 2,500 km, from the arid northeast to the savannahs of the southwest (Strauss et al., 2020). Rock art, presumably contemporaneous with the Itaparica Tradition, is common in northeastern and central Brazil, with identical motifs occurring more than 1,500 km apart (Neves et al., 2012). The evidence shows that during this timeframe human populations in NEB were part of a pan-continental network of shared goods and information (Bueno and Isnardis, 2018).

The geographical extent of the Itaparica Tradition was only surpassed in the New World by the Clovis Tradition in North America. However, while the latter was an ephemeral phenomenon lasting no longer than a few centuries, the former was a highly resilient techno-complex. The Itaparica Tradition endured for almost five millennia until it came to an end at around 8,000 yrs BP. At this point, a process of fragmentation and fission is evident (Bueno and Isnardis, 2018), bringing to an end the existence of pan-continental lithic techno-complexes in Brazil. Archaeological units of comparable magnitude would only resurge thousands of years later at around 2,000 yrs BP when pottery produced by the ancestral of Jê (Aratu Tradition) and Tupi-Guarani (Tupiguarani Tradition) groups finally arrived in the region (Martin, 2013; Gregorio de Souza et al., 2020).

In NEB, the earliest appearance of pottery occurs at ca. 4,000 yrs BP as localized occurrences along the major rivers such as the São Francisco River. It is only after ca. 2,000 yrs BP, however, with the arrival of pottery-making groups from central Brazil and the Amazon, that horticulturalist practices became ubiquitous in the region. These populations adapted their cultivation techniques and subsistence strategies to the semi-arid environments, thriving until the arrival of the European invader. The ethnography of the region is testimony of their success, as represented by culturally rich, linguistically diverse and demographically dense populations.

The period between consolidated regional foragers during the Early Holocene (Itaparica) and the ascension of Late Holocene horticulturalists (Aratu e Tupigurani) is poorly documented for the NEB region. This same pattern, with minor local variants, is also known to central Brazil, the Amazon and the Andes (but not the Southern Cone). This archaeological silence is reflected in the aforementioned reduction in radiocarbon dates across large regions of South America. Under the assumption that radiocarbon dates from archaeological sites are a proxy for demographic density, this pattern reflects depopulation of large areas between ca. 8,000 and 5,000 yrs BP. This pattern is unlikely to be driven by climate changes in NEB, as the region faced wetter conditions during this same period.

Generalized climatic deterioration in South America during the Middle Holocene in the form of drier/colder periods or an increase of climatic instability was proposed as the main driver of the demographic deflation inferred from the radiocarbon data (Araujo et al., 2005; Riris, Arroyo-Kalin, 2019). However, NEB deviates from this general pattern in significant ways. Far from being a climatically stressful time for human population, our data show that the Middle Holocene in NEB was a phase of ameliorated climate with increased precipitation. NEB would then constitute an ecological refugium for populations from neighboring regions struggling with worsening climatic conditions. However, the radiocarbon dates compiled in this study (Fig. S6) demonstrate that far from attracting human groups, the region instead went through the same demographic collapse inferred for other regions.

Climate-free ecological models propose that after the initial settlement of the continent, as populations grow and spread, maximum carrying capacity would be achieved by the beginning of

the Middle Holocene. Without food-producing techniques the demographic expansion of these populations would stabilize for the coming three thousand years until cultivation became sufficiently widespread to significantly increase carrying capacity all over the continent (Goldberg et al., 2016). Therefore, the demographic evolution of human populations in South America would not be conditioned by climatic changes but instead by its internal dynamics. The diverse post-colonial societies that are known to have thrived in the harsh environment of the caatinga are testimony of the efficiency of adaptive strategies to overcome unfavorable climatic conditions and natural resource limitations.

6. Conclusion

Our multi-proxy study from Chapada do Apodi shows contrasting environmental and paleoclimatic conditions during the Meghalayan period when compared with the previous period, from ~11,000 to 4,200 yrs BP. The first period was characterized by denser vegetation (predominance of savanna), higher rainfall amounts and thicker soil cover above the cave system, while the Meghalayan period is marked in NEB by a decreased rainfall amount, sparse vegetation (predominance of caatinga) and reduced soil layer above the cave. In addition, a more seasonal climate was established in the region when the ITCZ-related rainfall became more limited to the March to May period. These changes occur abruptly from 4,800 to 4,200 yrs BP, coincident with the reversion of the insolation tendency at about 5,000 yrs BP in South America. Hence, we conclude that the semi-arid to arid region of NEB has a very sensitive ecosystem, with unknown thresholds, that can lead to an abrupt environmental change. That should clearly be a matter of concern in terms of future climate scenarios.

These results provide valuable information to understand how changes in precipitation affect the resilience of ecosystems in the region and to better constrain model projections of future precipitation and vegetation changes. This is particularly critical in a region such as NEB, where aridification is underway due to current climate change. Our climatic proxies for NEB do not seem to corroborate an association between climatic change and demographic events in South America during the Middle Holocene. While the climate in the region is shown to follow a unique trajectory with no counterparts elsewhere in the country, the overall demographic course is virtually identical to the well-established curve over the rest of South America, characterized by population deflation during Middle Holocene.

Authors contributions

G.U. and F.W.C designed the experiment, performed isotopic analysis and prepared the manuscript with help from the co-authors; F.W.C. directed the project; R.V.S. coordinated the laboratory procedures for strontium isotope analysis; A.O.S., N.M.S. and V.F.N. contributed with the paleoclimate interpretations; H.W. and L.C.R.P. helped with the radiocarbon dating; M.V. helped with the interpretation and revision of the manuscript; A.S. and A.C.B. helped with archaeological data compilation and related interpretations; C.C.F.G. and A.O.S provided the OSL ages; F.R.D.A. provided and interpreted the mineralogical analysis; H.Z. helped with U/Th analysis and revision of the manuscript, and H.C. and R.L.E. coordinated the laboratory procedures for U/Th analysis.

Data availability

The dataset generated as part of this study will be available in the PANGAEA.

Declaration of competing interest

The authors declare that they have no known competing financial interests or personal relationships that could have appeared to influence the work reported in this paper.

Acknowledgments

We thank Christian Millo, Alyne Barros M. Lopes and Osmar Antunes (LES-IGc-USP, Brazil), and Luiz Mancini (LAIS-IGc-UNB, Brazil) for their support during the analyses, André Zular (IGc-USP, Brazil) for support during the field trip and grain-size analysis, Johan Etourneau (Université de Bordeaux, France) for comments about this paper. We are grateful to Professor Dr. Francisco Hilário Bezerra (UFRN, Brazil) and A.N.P., Brazil for aerial images and Carlos Mazocca (IGc-USP, Brazil) for images editing. This work was supported by the FAPESP, Brazil through PIRE NSF-FAPESP [2017/50085−3 to F.W.C], as well as the fellowships to G.U. [2020/02737−4]. V.F.N [2016/15807−5], A.S. [2017/16451−2] and A.C.B. [2019/12981−2], and the regular research grant [2019/15914−4 to A.S.]. The NSF, United States support through grants [AGS-1303828 and OISE-1743738] to MV and 1103403 to R.L.E and H.C. is acknowledged. The NSFC, China support through grant [NSFC 41888101] to H.C. is acknowledged. N.M.S. acknowledges the support of CNPq, Brazil [Grants 423573/2018−7; 308769/2018−0] and CAPES, Brazil [Grant 88887.310301/2018−00]. G.U. is grateful to CAPES for the PhD and PosDoc fellowships through the Programa de Pós-Graduação em Geoquímica e Geotectônica at Universidade de São Paulo, Brazil.

Appendix A. Supplementary data

Supplementary data to this article can be found online at https://doi.org/10.1016/j.quascirev.2020.106655.

References

Ab'Saber, A.N., 1974. O domínio morfoclimático semi-árido das Caatingas brasileiras. Geomorfologia 43, 1−39.
Aitken, M.J., 1998. An Introduction to Optical Dating. Oxford University Press., London.
Alley, R.B., et al., 2003. Abrupt climate change. Science 299, 2005−2010. https://doi.org/10.1126/science.1081056.
ANA − Agência Nacional de Águas, 2013. Sistema Nacional de Informações sobre Recursos Hídricos. http://www.snirh.gov.br/hidroweb/apresentacao. (Accessed 25 July 2020).
Angelim, L.A.A., Medeiros, V.C., Nesi, J.R., 2006. Programa Geologia do Brasil − PGB. Projeto Geologia e Recursos Minerais do Estado do Rio Grande do Norte. Mapa geológico do Estado do Rio Grande do Norte. Escala. 1:500.000. Recife: CPRM/FAPERN. 1 mapa color. http://www.cprm.gov.br/publique/media/geologia_basica/cartografia_regional/mapa_rio_grande_norte.pdf. (Accessed 2 February 2019).
Araujo, A.G.M., Neves, W.A., Piló, L.B., Atui, J.P.V., 2005. Holocene dryness and human occupation in Brazil during the "archaic gap. Quat. Res. 64 (3), 298−307. https://doi.org/10.1016/j.yqres.2005.08.002.
Arz, H.W., Pätzold, J., Wefer, G., 1999. The deglacial history of the western tropical Atlantic as inferred from high resolution stable isotope records off northeastern Brazil. Earth Planet Sci. Lett. 167, 108−117. https://doi.org/10.1016/S0012-821X(99)00025-4.
Ayalon, A., Bar-Matthews, M., Kaufman, A., 1999. Petrography, strontium, barium and uranium concentrations, and strontium and uranium isotope ratios in speleothems as palaeoclimatic proxies: soreq Cave, Israel. Holocene 9, 715−722. https://doi.org/10.1191/095968399673664163.
Baker, et al., 1997. Elevated and variable values of 13C in speleothems in a British cave system. Chem. Geol. 136, 263−270. https://doi.org/10.1016/S0009-2541(96)00129-5.
Banner, et al., 2004. Radiogenic isotopes: systematics and applications to earth surface processes and chemical stratigraphy. Earth Sci. Rev. 65, 141−194. https://doi.org/10.1016/S0012-8252(03)00086-2.
Behling, H., et al., 2000. Late Quaternary vegetational and climate dynamics in northeastern Brazil, inferences from marine core GeoB 3104-1. Quat. Sci. Rev. 19, 981−994. https://doi.org/10.1016/S0277-3791(99)00046-3.
Bento, D.M., et al., 2011. Mapeamento, caracterização ambiental e relevância do

patrimônio espeleológico de Felipe Guerra/RN. In: 31° Congresso Brasileiro de Espeleologia, Ponta Grossa-PR. ANAIS, Ponta Grossa, pp. 485–499.
Berger, A., Loutre, M.F., 1991. Insolation values for the climate of the last 10 million of years. Quat. Sci. Rev. 10, 297–317. https://doi.org/10.1016/0277-3791(91)90033-Q.
Berkelhammer, M., et al., 2012. An abrupt shift in the Indian monsoon 4000 years ago. Geophys. Monogr. 198, 75–88. https://doi.org/10.1029/2012GM001207.
Bertotti, G., et al., 2017. Fracturing and fluid-flow during post-rift subsidence in carbonates of the jandaıra formation, Potiguar Basin, NE Brazil. Basin Res. 29, 836–853. https://doi.org/10.1111/bre.12246.
Beuchle, R., et al., 2015. Land cover changes in the Brazilian Cerrado and Caatinga biomes from 1990 to 2010 based on a systematic remote sensing sampling approach. Appl. Geogr. 58, 116–127. https://doi.org/10.1016/j.apgeog.2015.01.017.
Bini, M., et al., 2019. The 4.2 kaBP Event in the Mediterranean region: an overview. Clim. Past 15, 555–577. https://doi.org/10.5194/cp-15-555-2019.
Blaauw, M., 2010. Methods and code for 'classical' age-modelling of radiocarbon sequences. Quat. Geochronol. 5, 512–518. https://doi.org/10.1016/j.quageo.2010.01.002.
Bond, G., et al., 1997. A pervasive millennial-scale cycle in north atlantic Holocene and glacial climates. Science 278, 1257–1266. https://doi.org/10.1126/science.278.5341.1257.
Booth, R.K., et al., 2005. A severe centennial-scale drought in midcontinental North America 4200 years ago and apparent global linkages. Holocene 15 (3), 321–328. https://doi.org/10.1191/0959683605hl825ft.
Braconnot, P., et al., 2008. Monsoon response to changes in Earth's orbital parameters: comparisons between simulations of the Eemian and of the Holocene. Clim. Past 4, 281–294. https://doi.org/10.5194/cp-4-281-2008.
Breitenbach, S.F.M., et al., 2012. COnstructing proxy records from age models (COPRA). Clim. Past 8, 1765–1779. https://doi.org/10.5194/cp-8-1765-2012.
Bueno, L., Isnardis, A., 2018. Peopling central Brazilian plateau at the onset of the Holocene: Building territorial histories. Quat. Int. 473, 144–160. https://doi.org/10.1016/j.quaint.2018.01.006.
Burns, S.J., et al., 2002. A 780-year annually resolved record of Indian Ocean monsoon precipitation from a speleothem from south Oman. J. Geophys. Res. 107 (D20), 4434. https://doi.org/10.1029/2001jd001281.
Buso Junior, A.A., et al., 2019. Paleovegetation and paleoclimate dynamics during the last 7000 years in the Atlantic forest of Southeastern Brazil based on palynology of a waterlogged sandy soil. Rev. Palaeobot. Palynol. 264, 1–10. https://doi.org/10.1016/j.revpalbo.2019.02.002.
Cabrol, P., Coudray, J., 1982. Climatic fluctuations influence the genesis and diagenesis of carbonate speleothems in southwestern France. Natl. Speleo. Soc. Bull. 44, 112–117.
Calegari, M.R., et al., 2017. Potential of soil phytoliths, organic matter and carbon isotopes for small-scale differentiation of tropical rainforest vegetation: a pilot study from the campos nativos of the Atlantic Forest in Espírito Santo State (Brazil). Quat. Int. 437 (B), 156–164. https://doi.org/10.1016/j.quaint.2016.01.023.
Cheng, H., et al., 2013a. Climate change patterns in Amazonia and biodiversity. Nat. Commun. 4, 1411. https://doi.org/10.1038/ncomms2415.
Cheng, H., et al., 2013b. Improvements in 230Th dating, 230Th and 234U half-life values and U–Th isotopic measurements by multi-collector inductively coupled plasma mass spectrometry. Earth Planet. Sci. Lett. 371– 372, 82–91. https://doi.org/10.1016/j.epsl.2013.04.006.
Cheng, H., et al., 2015. The climate variability in northern Levant over the past 20,000 years. Geophys. Res. Lett. 42, 8641–8650. https://doi.org/10.1002/2015GL065397.
Choquette, P.W., James, N.P., 1988. Introduction. In: James, N.P., Choquette, P.W. (Eds.), Paleokarst. Springer-Verlag New York, pp. 1–8. https://doi.org/10.1007/978-1-4612-3748-8.
Cooke, et al., 2003. Precise timing and rate of massive late Quaternary soil denudation. Geol. 31 (10), 853–856. https://doi.org/10.1130/G19749.1.
Cruz Jr., F.W., et al., 2005. Insolation-driven changes in atmospheric circulation over the past 116,000 years in subtropical Brazil. Nature 434, 63–66. https://doi.org/10.1038/nature03365.
Cruz Jr., F.W., et al., 2006. A stalagmite record of changes in atmospheric circulation and soil processes in the Brazilian subtropics during the Late Pleistocene. Quat. Sci. Rev. 25, 2749–2761. https://doi.org/10.1016/j.epsl.2006.06.019.
Cruz, F.W., et al., 2009. Orbitally driven east–west antiphasing of South American precipitation. Nat. Geosci. 2, 210–214. https://doi.org/10.1038/ngeo444.
Cruz Júnior, F.W., 1996. Sistemas Deposicionais, Geomorfologia e Geologia Estrutural de uma área na região de Felipe Guerra, Sudoeste da Bacia Potiguar. Relatório de Graduação, UFRN, p. 120. In Portuguese).
Dang, S., et al., 2020. El Niño/Southern Oscillation during the 4.2 ka event recorded by growth rates of corals from the North South China Sea. Acta Oceanol. Sin. 39 (1), 110–117. https://doi.org/10.1007/s13131-019-1520-5.
De Oliveira, P.E., et al., 1999. Late Pleistocene-Holocene climatic and vegetational history of the Brazilian caatinga: the fossil dunes of the middle São Francisco River. Palaeogeogr. Palaeoclimatol. Palaeoecol. 152, 319–337. https://doi.org/10.1016/S0031-0182(99)00061-9.
Denniston, R.F., et al., 2017. Decoupling of monsoon activity across the northern and southern Indo-Pacific during the Late Glacial. Quat. Sci. Rev. 176, 101–105. https://doi.org/10.1016/j.quascirev.2017.09.014.
Dixit, Y., Hodell, D.A., Petrie, C.A., 2014. Abrupt weakening of the summer monsoon in northwest India ~4100 yr ago. Geology 42 (4), 339–342. https://doi.org/10.1130/G35236.1.
Dreybrodt, W., 2008. Evolution of the isotopic composition of carbon and oxygen in a calcite precipitating H2O-CO2-CaCO3 solution and the related isotopic composition of calcite in stalagmites. Geochem. Cosmochim. Acta 72, 4712–4724. https://doi.org/10.1016/j.gca.2008.07.022.
Dreybrodt, W., Scholz, D., 2011. Climatic dependence of stable carbon and oxygen isotope signals recorded in speleothems: from soil water to speleothem calcite. Geochem. Cosmochim. Acta 75, 734–753. https://doi.org/10.1016/j.gca.2010.11.002.
Dupont, L.M., et al., 2010. Two-step vegetation response to enhanced precipitation in Northeast Brazil during Heinrich event 1. Global Change Biol. 16, 1647–1660. https://doi.org/10.1111/j.1365-2486.2009.02023.x.
Erasmi, S., et al., 2009. Inter-annual variability of the normalized difference vegetation index over northeast Brazil and its relation to rainfall and El Niño southern oscillation. Geo-oko 30, 185–206.
Fairchild, I.J., Baker, A., 2012. Speleothem Science: from Process to Past Environments. Wiley-Blackwell, Chichester. https://doi.org/10.1002/9781444361094.
Fairchild, I.J., et al., 2000. Controls on trace element (Sr–Mg) compositions of carbonate cave waters: implications for speleothem climatic records. Chem. Geol. 166, 255–269. https://doi.org/10.1016/S0009-2541(99)00216-8.
Fairchild, I.J., et al., 2006. Modification and preservation of environmental signals in speleothems. Earth Sci. Rev. 75, 105–153. https://doi.org/10.1016/j.earscirev.2005.08.003.
Feng, W., et al., 2012. Oxygen isotopic fractionation between drip water and speleothem calcite: a 10-year monitoring study, central Texas, USA. Chem. Geol. 304–305, 53–67. https://doi.org/10.1016/j.chemgeo.2012.02.004.
Fisher, D.A., 2011. Connecting the Atlantic-sector and the north Pacific (Mt Logan) ice core stable isotope records during the Holocene: the role of El Nino. Holocene 21 (7), 1117–1124. https://doi.org/10.1177/0959683611400465.
Frisia, S., et al., 2002. Aragonite–calcite relationships in speleothems (Grotte de Clamouse, France): environment, fabrics, and carbonate geochemistry. J. Sediment. Res. 72 (5), 687–699. https://doi.org/10.1306/020702720687.
Frumkin, A., Stein, M., 2004. The Sahara-East Mediterranean dust and climate connection revealed by strontium and uranium isotopes in a Jerusalem speleothem. Earth Planet Sci. Lett. 217, 451–464. https://doi.org/10.1016/S0012-821X(03)00589-2.
Galbraith, R.F., et al., 1999. Optical dating of single and multiple grains of quartz from Jinmium rock shelter, northern Australia: Part I, Experimental design and statistical models. Archaeometry 41, 361–364. https://doi.org/10.1111/j.1475-4754.1999.tb00987.x.
Gen, X.G., et al., 2020. Modulation of the relationship between ENSO and its combination mode by the atlantic multidecadal oscillation. J. Clim. 33, 4679–4695. https://doi.org/10.1175/JCLI-D-19-0740.1.
Genty, D., et al., 2003. Precise dating of Dansgaard-Oeschger climate oscillations in western Europe from stalagmite data. Nature 421, 833–838. https://doi.org/10.1038/nature01391.
Goldberg, A., Mychajliw, A.M., Hadly, E.A., 2016. Post-invasion demography of prehistoric humans in South America. Nature 532, 232–235. https://doi.org/10.1038/nature17176.
González-Lemos, S., Jiménez-Sánchez, M., Stoll, H.M., 2015. Sediment transport during recent cave flooding events and characterization of speleothem archives of past flooding. Geomorphology 228, 87–100. https://doi.org/10.1016/j.quascirev.2015.06.002.
Gražulis, S., et al., 2009. Crystallography Open Database – an open-access collection of crystal structures. J. Appl. Crystallogr. 42, 726–729. https://doi.org/10.1107/S0021889809016690.
Gregorio de Souza, J., Alcaina Mateos, J., Madella, M., 2020. Archaeological expansions in tropical South America during the late Holocene: assessing the role of demic diffusion. PloS One 15 (4), e0232367. https://doi.org/10.1371/journal.pone.0232367.
Hendy, C.H., 1971. The isotopic geochemistry of speleothems I. The calculation of the effects of different modes of formation on the isotopic composition of speleothems and their applicability as palaeoclimatic indicators. Geochem. Cosmochim. Acta 85, 801–824.
Herman, E.K., Toran, L., White, W.B., 2012. Clastic sediment transport and storage in fluviokarst aquifers: an essential component of karst hydrogeology. Carbonates Evaporites 27, 211–241. https://doi.org/10.1007/s13146-012-0112-7.
Hogg, A.G., et al., 2013. SHCAL13 Southern Hemisphere calibration, 0–50,000 years cal BP. Radiocarbon 55 (4), 889–1903. https://doi.org/10.2458/azu_js_rc.55.16783.
Hori, M., et al., 2013. Prior calcite precipitation and source mixing process influence Sr/Ca, Ba/Ca and 87Sr/86Sr of a stalagmite developed in southwestern Japan during 18.0 4.5 ky. Chem. Geol. 347, 190–198. https://doi.org/10.1016/j.chemgeo.2013.03.005.
INMET Instituto Nacional de Meteorologia – data from 1961-1990. Banco de Dados Meteorológicos para Ensino e Pesquisa. http://www.inmet.gov.br/(accessed 2019 Jun 15).
Isola, I., et al., 2019. The 4.2 ka event in the central Mediterranean: new data from a Corchia speleothem (Apuan Alps, central Italy). Clim. Past 15, 135–151. https://doi.org/10.5194/cp-15-135-2019.
Jaeschke, A., et al., 2007. Coupling of millennial-scale changes in sea surface temperature and precipitation off northeastern Brazil with high-latitude climate shifts during the last glacial period. Paleoceanography 22, PA4206. https://doi.org/10.1029/2006PA001391.
Jennerjahn, T.C., et al., 2004. Asynchronous terrestrial and marine signals of climate

change during Heinrich Events. Science 306, 2236–2239. https://doi.org/10.1126/science.1102490.
Johnson, K.R., et al., 2006. Seasonal trace-element and stable isotope variations in a Chinese speleothem: the potential for high resolution paleomonsoon reconstruction. Earth Planet Sci. Lett. 244, 394–407. https://doi.org/10.1016/j.epsl.2006.01.064.
Jones, B., Zheng, E., Li, L., 2018. Growth and development of notch speleothems from Cayman Brac, British West Indies: response to variable climatic conditions over the last 125,000 years. Sediment. Geol. 373, 210–227. https://doi.org/10.1016/j.sedgeo.2018.06.005.
Kaniewski, D., et al., 2017. Climate change and water management in the biblical city of Dan. Sci. Adv. 3, e1700954 https://doi.org/10.1126/sciadv.1700954.
Leal, I.R., et al., 2005. Changing the course of biodiversity conservation in the caatinga of northeastern Brazil. Conserv. Biol. 19 (3), 701–706. https://doi.org/10.1111/j.1523-1739.2005.00703.x.
Ledru, M.-P., et al., 2002. Tropical climates in the game of two hemispheres revealed by abrupt climatic change. Geology 30 (3), 275–278. https://doi.org/10.1130/0091-7613(2002)030<0275:TCITGO>2.0.CO;2.
Ledru, M.-P., et al., 2006. Millenial-scale climatic and vegetation changes in a northern cerrado (northeast, Brazil) since the last glacial maximum. Quat. Sci. Rev. 25, 1110–1126. https://doi.org/10.1016/j.quascirev.2005.10.005.
Ledru, M.-P., Mourguiart, P., Riccomini, C., 2009. Related changes in biodiversity, insolation and climate in the Atlantic rainforest since the last interglacial. Palaeogeogr. Palaeoclimatol. Palaeoecol. 271, 140–152. https://doi.org/10.1016/j.palaeo.2008.10.008.
Li, et al., 2005. 87Sr/86Sr and Sr/Ca in speleothems for paleoclimate reconstruction in Central China between 70 and 280 kyr ago. Geochem. Cosmochim. Acta 69 (16), 3933–3937. https://doi.org/10.1016/j.gca.2005.01.009.
Liu, F., Feng, Z., 2012. A dramatic climatic transition at ~4000 cal. yr BP and its cultural responses in Chinese cultural domains. Holocene 22, 1181–1197. https://doi.org/10.1177/0959683612441839.
Lourdeau, A., 2015. Lithic technology and prehistoric settlement in central and northeast Brazil: definition and spatial distribution of the Itaparica technocomplex. PaleoAmerica 1 (1), 52–67. https://doi.org/10.1179/2055556314Z.0000000005.
Maksic, J., et al., 2018. Simulation of the Holocene climate over South America and impacts on the vegetation. Holocene 1–13. https://doi.org/10.1177/0959683618810406.
Martin, G., 2013. Pré-História Do Nordeste Do Brasil, 5° edition. Editora Universitária UFPE.
Mayle, F.E., Burbridge, R., Killeen, T.J., 2000. Millennial-scale dynamics of southern amazonian rain forests. Science 290, 2291–2294. https://doi.org/10.1126/science.290.5500.2291.
McArthur, J.M., Howarth, R.J., Bailey, T.R., 2001. Strontium isotope stratigraphy: LOWESS version 3: Best fit to the marine Sr-isotope curve for 0–509 ma and accompanying look-up table for deriving numerical age. J. Geol. 109 (2), 155–170. https://doi.org/10.1086/319243.
McDermott, F., 2004a. Palaeo-climate reconstruction from stable isotope variations in speleothems: a review. Quat. Sci. Rev. 23, 901–918. https://doi.org/10.1016/j.quascirev.2003.06.021.
Melo, A.C.C., et al., 2016. Rift fault geometry and evolution in the Cretaceous Potiguar Basin (NE Brazil) based on fault growth models. J. South Am. Earth Sci. 71, 96–107. https://doi.org/10.1016/j.jsames.2016.07.006.
Merino, E., Banerjee, A., 2008. Terra Rossa genesis, implications for karst, and eolian dust: a geodynamic thread. J. Geol. 116, 62–75. https://doi.org/10.1086/524675.
Meyer, K.W., et al., 2014. Interpretation of speleothem calcite δ13C variations: evidence from monitoring soil CO2, drip water, and modern speleothem calcite in central Texas. Geochem. Cosmochim. Acta 142, 281–298. https://doi.org/10.1016/j.gca.2014.07.027.
Mickler, P., et al., 2004. Stable isotope variations in modern tropical speleothems: evaluating equilibrium vs. kinetic isotope effects. Geochem. Cosmochim. Acta 68, 4381–4393. https://doi.org/10.1016/j.gca.2004.02.012.
Miller, E.K., Blum, J.D., Friedland, A.J., 1993. Determination of soil exchangeable-cation loss and weathering rates using Sr isotopes. Nature 362, 3–6. https://doi.org/10.1038/362438a0.
Montade, V., et al., 2014. Stability of a Neotropical microrefugium during climatic instability. J. Biogeogr. 41, 1215–1226. https://doi.org/10.1111/jbi.12283.
Mota, L., Scheel-Ybert, R., 2019. Landscape and firewood use in Toca do Boqueirão da Pedra Furada (Piauí, Brazil) during early and Mid-Holocene. J.Archaeo. Sci.: Report 23, 281–290. https://doi.org/10.1016/j.jasrep.2018.10.034.
Mulitza, S., et al., 2017. Synchronous and proportional deglacial changes in Atlantic meridional overturning and northeast Brazilian precipitation. Paleoceanography 32. https://doi.org/10.1002/2017PA003084.
Neves, W.A., Araujo, A.G.M., Bernardo, D.V., Kipnis, R., Feathers, J.K., 2012. Rock art at the pleistocene/holocene Boundary in eastern south America. PloS One 7 (2), e32228. https://doi.org/10.1371/journal.pone.0032228.
Novello, V.F., et al., 2017. A high-resolution history of the south American monsoon from last glacial maximum to the Holocene. Sci. Rep. 7, 44267. https://doi.org/10.1038/srep44267.
Novello, V.F., et al., 2019. Vegetation and environmental changes in tropical South America from the last glacial to the Holocene documented by multiple cave sediment proxies. Earth Planet Sci. Lett. 524, 115717. https://doi.org/10.1016/j.epsl.2019.115717.
Novello, et al., 2020. δ13C values in stalagmites from tropical South America for the last two millennia. Earth Syst. Sci. Data Discuss. https://doi.org/10.5194/essd-2020-184 (submitted for publication).
Paquette, J., Reeder, R.J., 1990. Single-crystal X-ray structure refinements of two biogenetic magnesian calcite crystals. Am. Mineral. 75, 1151–1158.
Pessenda, L.C.R., Camargo, P.B., 1991. Datação radiocarbônica de amostras de interesse arqueológico e geológico por espectrometria de cintilação líquida de baixa radiação de fundo. Quím. Nova 14 (2), 98–103.
Pessenda, L.C.R., et al., 1996. Natural radiocarbon measurements in Brazilian soils developed on basic rocks. Radiocarbon 38 (2), 203–208. https://doi.org/10.1017/S0033822200017574.
Pessenda, L.C.R., et al., 2010. Late Pleistocene and Holocene vegetation changes in northeastern Brazil determined from carbon isotopes and charcoal records in soils. Palaeogeogr. Palaeoclimatol. Palaeoecol. 297 (3–4), 597608. https://doi.org/10.1016/j.palaeo.2010.09.008.
Pessoa-Neto, O.C., 2003. Estratigrafia de sequências da plataforma mista neogênica na Bacia Potiguar, margem equatorial brasileira. Rev. Bras.Geoci. 33 (3), 263–278.
Pinaya, J.D., et al., 2019. Brazilian montane rainforest expansion induced by Heinrich Stadial 1 event. Sci. Rep. 9, 17912. https://doi.org/10.1038/s41598-019-53036-1.
Pokroy, B., et al., 1989. Atomic structure of biogenic aragonite. Chem. Mater. 19, 3244–3251. https://doi.org/10.1021/cm070187u.
Porpino, K.O., Júnior, V.S., Santos, M.F.C.F., 2009. Lajedo de Soledade, Apodi, state of Rio Grande do Norte – a remarkable megafauna site from northeastern Brazil. In: Winge, M., et al. (Eds.), SIGEP - Sítios Geológicos e Paleontológicos do Brasil. 2°, vol. 2. CPRM, Brasília, pp. 403–412.
Prado, D., 2003. As caatingas da América do Sul. In: Leal, I.R., Tabarelli, M., Silva, J.M.C. (Eds.), Ecologia e conservação da Caatinga. Editora Universitária, Universidade Federal de Pernambuco, Recife, Brasil, pp. 3–73.
Prado, L.F., Wainer, I., Chiessi, C.M., 2013. Mid-holocene PMIP3/CMIP5 model results: intercomparison for the south American monsoon system. Holocene 23 (12), 1915–1920. https://doi.org/10.1177/0959683613505336.
Prescott, J.R., Stephan, L.G., 1982. The contribution of cosmic radiation to the environmental dose for thermoluminescence dating. PACT 6, 17–25. https://doi.org/10.1016/1350-4487(94)90086-8.
Ran, M., Chen, L., 2019. The 4.2 ka BP climatic event and its cultural responses. Quat. Int. 521, 158–167. https://doi.org/10.1016/j.quaint.2019.05.030.
Ratter, J.A., Ribeiro, J.F., Bridgewater, S., 1997. The Brazilian Cerrado vegetation and threats to its biodiversity. Ann. Bot. (Lond.) 80, 223–230.
Riris, P., Arroyo-Kalin, M., 2019. Widespread population decline in South America correlates with mid-Holocene climate change. Sci. Rep. 9, 6850. https://doi.org/10.1038/s41598-019-43086-w.
Schubert, B.A., Jahren, A.H., 2012. The effect of atmospheric CO2 concentration on isotope fractionation in C3 land plants. Geochem. Cosmochim. Acta 96, 29–43. https://doi.org/10.1016/j.gca.2012.08.003.
Silva, O.L., et al., 2017. Karst landforms revealed at various scales using LiDAR and UAV in semi-arid Brazil: consideration on karstification processes and methodological constraints. Geomorphology 295, 611–630. https://doi.org/10.1016/j.geomorph.2017.07.025.
Embrapa Solos Empresa Brasileira de Pesquisa Agropecuária, 1971-2006. Levantamento Exploratório-Reconhecimento de Solos do Estado do Rio Grande do Norte (MA/EMBRAPA/SUDENE,1971) solos.uep.cnps.embrapa.br (accessed Feb. 01 2020).
Sonneveld, E.J., Visser, J.W., 1975. Automatic collection of powder data from photographs. J. Appl. Crystallogr. 8, 1–7. https://doi.org/10.1107/S0021889875009417.
Strauss, A., et al., 2020. The archaeological record of lagoa santa (east-Central Brazil): from the late pleistocene to historical times. In: AulerA, S., Pessoa, P. (Eds.), Lagoa Santa Karst: Brazil's Iconic Karst Region. Cave and Karst Systems of the World. Springer, Cham. https://doi.org/10.1007/978-3-030-35940-9_12.
Strikis, N.M., et al., 2015. Timing and structure of mega-SACZ events during Heinrich stadial 1. Geophys. Res. Lett. 42, 5477–5484. https://doi.org/10.1002/2015GL064048.
Strikis, N.M., et al., 2018. South American monsoon response to iceberg discharge in the North Atlantic. P. Natl. Acad. Sci. USA 115 (15), 3788–3793. https://doi.org/10.1073/pnas.1717784115.
Stuiver, M., Polach, H.A., 1977. Discussion: reporting of 14C data. Radiocarbon 19 (3), 355–363.
Thompson, L.G., et al., 2002. Kilimanjaro ice core records: evidence of Holocene climate change in Tropical Africa. Science 298, 589–593. https://doi.org/10.1126/science.1073198.
Torrescano-Valle, N., Islebe, G.A., 2015. Holocene paleoecology, climate history and human influence in the southwestern Yucatan Peninsula. Rev. Palaeobot. Palynol. 217, 1–8. https://doi.org/10.1016/j.revpalbo.2015.03.003.
Toth, L.T., Aronso, R.B., 2019. The 4.2 ka event, ENSO, and coral reef development. Clim. Past 15, 105–119. https://doi.org/10.5194/cp-15-105-2019.
Utida, G., et al., 2019. Tropical South Atlantic influence on Northeastern Brazil precipitation and ITCZ displacement during the past 2300 years. Sci. Rep. 9, 1698. https://doi.org/10.1038/s41598-018-38003-6.
Veizer, J., 1989. Strontium isotopes in seawater through time. Annu. Rev. Earth Planet Sci. 17, 141–167.
Walker, M., et al., 2012. Formal subdivision of the Holocene series/epoch: a discussion paper by a working group of intimate (integration of ice-core, marine and terrestrial records) and the subcommission on quaternary stratigraphy (international commission on stratigraphy). J. Quat. Sci. 27 (7), 649–659. https://doi.org/10.1002/jqs.2565.
Walker, M., et al., 2018. Formal Ratification of the Subdivision of the Holocene

Series/Epoch (Quaternary System/Period): Two New Global Boundary Stratotype Sections and Points (GSSPs) and Three New Stages/subseries. Episodes. https://doi.org/10.18814/epiiugs/2018/018016.
Ward, B.M., et al., 2019. Reconstruction of Holocene coupling between the South America Monsoon System and local moisture variability from speleothem δ18O and 87Sr/86Sr records. Quat. Sci. Rev. 210, 51–63. https://doi.org/10.1016/j.quascirev.2019.02.019.
Weiss, H., 2016. Global megadrought, societal collapse and resilience at 4.2–3.9 ka BP across the Mediterranean and west Asia. PAGE 24, 62–63. https://doi.org/10.22498/pages.24.2.62.
Wentworth, C.K., 1922. A scale of grade and class terms for clastic sediments. J. Geol. 30 (5), 377–392.
Wintle, A.G., Murray, A.S., 2006. A review of quartz optically stimulated luminescence characteristics and their relevance in single-aliquot regeneration dating protocols. Radiat. Meas. 41 (4), 369–391. https://doi.org/10.1016/j.radmeas.2005.11.001.
Wong, C.I., Breecker, D.O., 2015. Advancements in the use of speleothems as climate archives. Quat. Sci. Rev. 127, 1–18. https://doi.org/10.1016/j.quascirev.2015.07.019.
Wortham, B.E., et al., 2017. Assessing response of local moisture conditions in central Brazil to variability in regional monsoon intensity using speleothem 87Sr/86Sr values. Earth Planet Sci. Lett. 463, 310–322. https://doi.org/10.1016/j.epsl.2017.01.034.
Zanchetta, G., et al., 2016. The so-called "4.2 event" in the central mediterranean and its climatic teleconnections. Alpine Medit. Quat. 29 (1), 5–17.
Zhang, Y., et al., 2017. Different precipitation patterns across tropical South America during Heinrich and Dansgaard-Oeschger stadials. Quat. Sci. Rev. 177, 1–9. https://doi.org/10.1016/j.quascirev.2017.10.012.
Zhang, H., et al., 2018. Hydroclimatic variations in southeastern China during the 4.2 ka event reflected by stalagmite records. Clim. Past 14, 1805–1817. https://doi.org/10.5194/cp-14-1805-2018.
Zhang, S., et al., 2020. Contrasting impacts of the 8.2- and 4.2-ka abrupt climatic events on the regional vegetation of the Hulun Lake region in north-eastern China. J. Quat. Sci. 35 (6), 831–840. https://doi.org/10.1002/jqs.3231.
Zhou, H., et al., 2009. Deglacial variations of Sr and 87Sr/86Sr ratio recorded by a stalagmite from central China and their association with past climate and environment. Chem. Geol. 268, 233–247. https://doi.org/10.1016/j.chemgeo.2009.09.003.
Zhu, X., Wang, S., Luo, W., 2011. Characteristics of strontium isotopes and their implications in the Qixing Cave of Guizhou, China. Chin. Sci. Bull. 56, 670–675. https://doi.org/10.1007/s11434-010-4337-3.
Ziese, M., et al., 2018. GPCC Full Data Daily Version.2018 at 1.0°: Daily Land-Surface Precipitation from Rain-Gauges Built on GTS-Based and Historic Data. https://doi.org/10.5676/DWD_GPCC/FD_D_V2018_100.
Zogbi, L.A., et al., 2013. Trapiá cave: exploration, survey, biology and geospeleology of the biggest cave of Rio Grande do Norte State. In: Filippi, M., Bosák, M., Bosak, P. (Eds.), Proceedings of the 16th International Congress of Speleology, vol. 2. Brno Czech Speleological Society, Prague, pp. 170–175.
Zular, A., et al., 2018. The effects of mid-Holocene fluvio-eolian interplay and coastal dynamics on the formation of dune-dammed lakes in NE Brazil. Quat. Sci. Rev. 196, 137–153. https://doi.org/10.1016/j.quascirev.2018.07.022.